



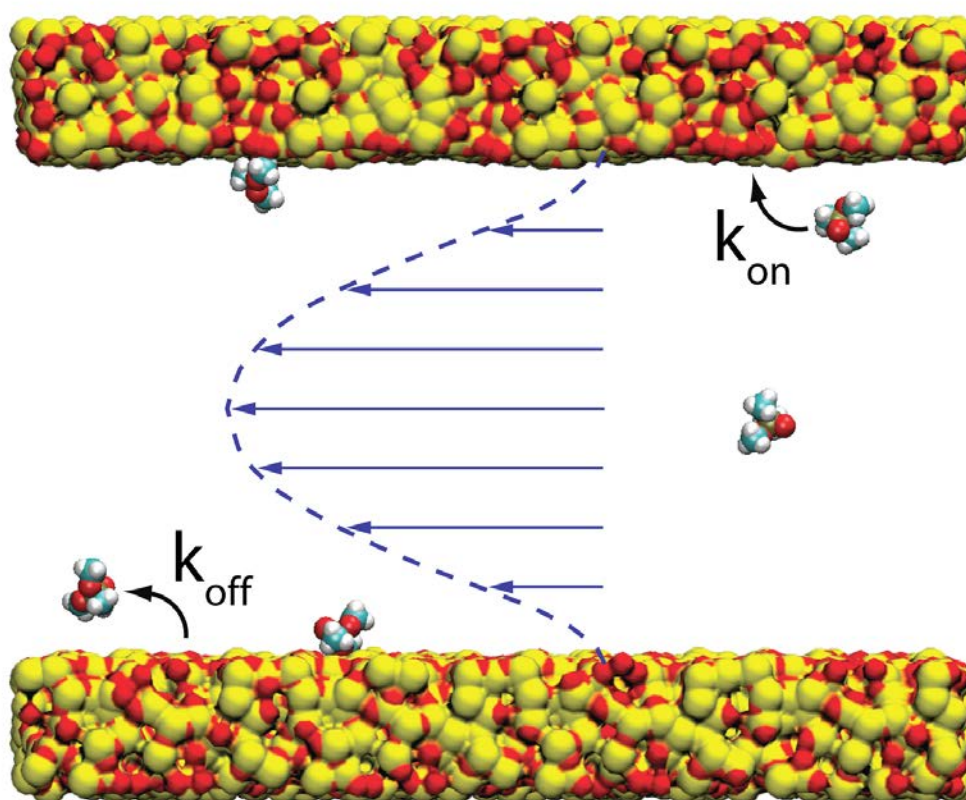
US Army Corps  
of Engineers®  
Engineer Research and  
Development Center

*Military Facilities Engineering Technology*

## **Molecular Modeling of Chem-Bio (CB) Contaminant Sorption/Desorption and Reactions in Chlorinated Water Systems**

Mark D. Ginsberg, Vincent F. Hock, Margaret Hurley, Frances Hill,  
Aleksei Aksimentiev, Rogan C. Carr, Jeffrey R. Comer, Kathryn A.  
Guy, Anne Beckman, Melixa Rivera-Sustache, Andy Nelson, Martin  
Page, Amanda Ehmann, and Vicki L. Van Blaricum

May 2012





# **Molecular Modeling of Chem-Bio (CB) Contaminant Sorption/Desorption and Reactions in Chlorinated Water Systems**

Mark D. Ginsberg, Vincent F. Hock, Kathryn A. Guy, Anne Beckman, Melixa Rivera-Sustache, Andy Nelson, Martin Page, Amanda Ehmann, and Vicki L. Van Blaricum

*Construction Engineering Research Laboratory (CERL)  
U.S. Army Engineer Research and Development Center (ERDC)  
2902 Newmark Drive  
Champaign, IL 61822*

Margaret Hurley

*U.S. Army Research Laboratory (ARL)  
2800 Powder Mill Road  
Adelphi, MD 20783*

Frances Hill

*Environmental Laboratory, Waterways Experiment Station  
U.S. Army Engineer Research and Development Center  
3909 Halls Ferry Road  
Vicksburg, MS 39180-6199*

Aleksei Aksimentiev, Rogan C. Carr, Jeffrey R. Comer

*University of Illinois at Urbana-Champaign  
College of Engineering  
Department of Physics  
1110 West Green Street  
Urbana, IL 61801-3080*

Final report

Approved for public release; distribution is unlimited.

Prepared for U.S. Army Corps of Engineers  
Washington, DC 20314-1000

Under P2 #150162, "Molecular Modeling of Chem-Bio (CB) Contaminant Sorption /  
Desorption and Reactions in Chlorinated Water Systems"

## Abstract

Army installations contain a high density of mission-critical buildings that require constant protection from accidental or deliberate contamination of water distribution systems. Current simulations of contaminant fate and transport in pipe systems do not accurately portray reality. The simulations assume pure hydraulic transport of contaminants and do not account for sorption of the contaminant on pipe walls. Additionally, subsequent reactions such as hydrolysis are not considered. These omissions reduce predictability of a contaminant's progression and effect in the distribution system. In addition, inadequate understanding of contaminant fate and transport may result in an unacceptable risk to mission readiness. However, performing laboratory tests for every known and emerging chemical or biological contaminant to obtain uptake and reaction parameters is not feasible with regard to time or cost investments. This report documents advances in molecular modeling predictions for the transport of contaminants using: the Nanoscale Molecular Dynamics program, the influence of bacterial biofilms on spore viability within a chlorinated water distribution system, the computational chemistry predictions of the rate of hydrolysis of a specific contaminant, and the inclusion of results into the predictive software, EPANet. This work opens the way for better vulnerability assessments, protection, real-time response, remediation, and planning.

**DISCLAIMER:** The contents of this report are not to be used for advertising, publication, or promotional purposes. Citation of trade names does not constitute an official endorsement or approval of the use of such commercial products. All product names and trademarks cited are the property of their respective owners. The findings of this report are not to be construed as an official Department of the Army position unless so designated by other authorized documents.

**DESTROY THIS REPORT WHEN NO LONGER NEEDED. DO NOT RETURN IT TO THE ORIGINATOR.**

# Table of Contents

<b>Abstract .....</b>	<b>ii</b>
<b>List of Figures and Tables.....</b>	<b>v</b>
<b>Preface.....</b>	<b>vii</b>
<b>Unit Conversion Factors .....</b>	<b>viii</b>
<b>1 Introduction.....</b>	<b>1</b>
1.1 Background.....	1
1.2 Objectives .....	3
1.3 Approach .....	3
1.4 Scope .....	4
1.5 Mode of technology transfer .....	4
<b>2 Experimental Program.....</b>	<b>5</b>
2.1 NAMD modeling.....	5
2.1.1 Thermodynamic derivation of the uptake parameter $\beta$ for EPANet.....	5
2.1.2 Derivation of the uptake time constant parameter $\Gamma$ for EPANet.....	6
2.2 Reaction rates with species in chlorinated water .....	7
2.3 Laboratory validation experiments.....	8
2.3.1 Prophos selection and analysis.....	8
2.3.2 Reactor vessels .....	9
2.3.3 Experimental set-up.....	10
2.4 Biofilm studies.....	11
2.4.1 <i>Bacillus globigii</i> preparation and enumeration .....	11
2.4.2 Experimental drinking water system.....	11
2.4.3 Bulk water and biofilm sampling.....	13
2.4.4 Bacterial enumerations .....	13
2.4.5 Water quality and biofilm characterization.....	14
2.4.6 Microscopy .....	14
<b>3 Results and Discussion.....</b>	<b>15</b>
3.1 Atomic resolution modeling – two phases.....	15
3.1.1 Phase 1: Atomic-scale features and molecule interaction with surfaces.....	15
3.1.2 Phase 2: Transport of molecules near surfaces .....	15
3.1.3 Nanoscale models of pipe surfaces.....	16
3.1.4 All-atom model of DMMP.....	17
3.1.5 Characterization of molecule-surface interactions .....	17
3.1.6 Model nanochannels .....	18
3.1.7 NAMD simulations of solute transport.....	19
3.1.8 Biomolecular transport in nanochannels .....	20
3.1.9 Continuum transport model for solutes in nanochannels.....	21

---

3.1.10	<i>Brownian dynamics transport model for solutes in nanochannels</i> .....	21
3.2	Laboratory validation experiments.....	22
3.3	Hydrolysis reaction rates and activation energy.....	26
3.4	Biofilm characterization and spore fate.....	30
<b>4</b>	<b>Implementation into EPANet MSX .....</b>	<b>37</b>
4.1	Simulations of fate and transport using EPANet MSX.....	38
<b>5</b>	<b>Future Research Efforts.....</b>	<b>40</b>
5.1	Water Integrated Security Test Laboratory.....	40
5.2	Secondary aerosol modeling.....	41
	<b>References .....</b>	<b>43</b>
	<b>Abbreviations.....</b>	<b>46</b>
	<b>Report Documentation Page</b>	

# List of Figures and Tables

## Figures

Figure 1. Graphic of chemical potential – the binding energy of a contaminant to the pipe surface.....	6
Figure 2. Optimized structure of an organophosphate.....	8
Figure 3. Reactor vessel (PVC) placed in tip-resistant PVC cup.....	9
Figure 4. Three pipe reactor vessels as assembled.....	10
Figure 5. Simulated PVC water distribution system: (A) Illustration of pipe loop system constructed with standard 2.5-cm PVC pipe and fittings. Three separate systems were constructed, each having a total length of 10 m, bulk phase volume of 17 L, operation temperature of approximately 25 °C, and a flow rate of 30 cm/sec; (B) The loop systems in operation—each was allowed to acclimate for 63 days as one unit then individually poised at 0.0, 0.5, and 1.0 mg/L free chlorine with sodium hypochlorite 3 days prior to the addition of <i>B. globigii</i> spores.....	12
Figure 6. Nanoscale models of pipe surfaces: (A) frictionless, (B) hydrophilic, (C) intermediate, and (D) hydrophobic .....	16
Figure 7. PMF calculations. The DMMP-surface PMF ( $W_{MS}$ ) was calculated as a function of the position of the DMMP over each surface. The silica surface is colored by the value of the PMF at that position of the surface. The DMMP is most attracted to the regions with the lowest PMF (shown in purple).....	18
Figure 8. Diagram of solute transport through a silica nanochannel. The average water profile calculated from the all-atom MD simulations is shown in blue. Solutes are transported by the flow of water through the channel and spontaneously bind and unbind on the channel surface. The binding constants ( $k_{off}$ and $k_{on}$ ) calculated from all-atom MD simulations were used as inputs to EPANet.....	19
Figure 9. Comparison of Brownian dynamics (BD) with all-atom molecular dynamics. (a) The concentration of DMMP bound to the surface of each nanochannel system is a function of time, wherein MD results for Surfaces A, B, C, and D (Figure 6) are shown as gray triangles, red diamonds, black squares, and blue circles, respectively, with averages over 25 unique BD trajectories for each nanochannel shown with lines of corresponding colors; (b) DMMP bound to Surface D as a function of position—MD results are on the left, while BD results are on the right. The BD captures the surface characteristics with atomic resolution detail.....	22
Figure 10. Atomic resolution BD simulation of DMMP advection through a 100 nm-long nanochannel for Surfaces C and D of Figure 6. A 10-mM concentration of DMMP is maintained on the left end of the channel, while the right end has an absorbing boundary. DMMP binds more strongly to the channel lined with Surface C than with Surface D; therefore, more time is required for DMMP to reach the end of the channel in the first case than for the second case, despite the identical water flow profiles.....	22
Figure 11. The 3-D depiction of Simulant P. View at left shows the molecule from the double-bonded oxygen side (easily seen by the intense red spot), and the right view is the obverse side. Polar regions are shown in red and blue; nonpolar regions are shown in green. The molecule is pinwheel shaped and is likely to have a single contact point with a nonpolar surface.....	25

Figure 12. The 3-D depiction of Agent V. Left view shows the molecule from the double-bonded oxygen side of the molecule (easily seen in the intense red spot); the view at right is the obverse side. Polar regions are shown in red and blue; nonpolar regions are shown in green. Notice that the nonpolar region at the bottom of the molecule is likely to have two contact points. ....	25
Figure 13. Clockwise from upper left: the step-wise hydrolysis of an organophosphonate via attack opposite the thiolate ligand. (The representative colors are yellow = phosphorus, dark yellow = sulfur; red = oxygen, blue = nitrogen, grey = carbon, and white = hydrogen.) ....	26
Figure 14. Changes in the energy of intermediate states in the hydrolysis pathway. ....	27
Figure 15. Susceptibility of heterotrophic bacteria and <i>B. globigii</i> spores to free chlorine in PVC pipe loop bulk water, presented as the log <sub>10</sub> of the total surviving fraction. Approximately 3.0 x 10 <sup>8</sup> viable <i>B. globigii</i> spores were added to each pipe loop system on Day Zero. Free chlorine in all systems was poised at 1.0 mg/L on Day 14. (Symbols: ♦ = heterotrophs, chlorine untreated; ◇ = <i>B. globigii</i> , chlorine untreated; ■ = heterotrophs, 0.5 mg/L free chlorine; □ = <i>B. globigii</i> , 0.5 mg/L free chlorine; ● = heterotrophs, 1.0 mg/L free chlorine; and ○ = <i>B. globigii</i> , 1.0 mg/L free chlorine. Data are means ± SD (n=3); some error bars are not visible due to size. ....	33
Figure 16. Susceptibility of heterotrophic bacteria and <i>B. globigii</i> spores to free chlorine in PVC pipe biofilm, presented as the log <sub>10</sub> of the total surviving fraction. Approximately 3.0 x 10 <sup>8</sup> <i>B. globigii</i> spores were added to each pipe loop system on day zero. Free chlorine in all systems was poised at 1.0 mg/L on day 14. Symbols: ♦ heterotrophs, chlorine untreated; ◇ <i>B. globigii</i> , chlorine untreated; ■ heterotrophs, 0.5 mg/L free chlorine; □ <i>B. globigii</i> , 0.5 mg/L free chlorine; ● heterotrophs, 1.0 mg/L free chlorine; and ○ <i>B. globigii</i> , 1.0 mg/L free chlorine. Data are means ± SD (n=3), some error bars are not visible due to size. ....	34
Figure 17. Hydrophilic water contamination would take a matter of hours, not days. Hydrophobic contamination would linger for a number of days. ....	39
Figure 18. Integrated water system protection. ....	40

## Tables

Table 1. Representative results for high-quality simulant and studied agent. ....	23
Table 2. Reaction rate constants for OP hydrolysis via hydroxide attack opposite the thiolate ligand. ....	28
Table 3. Reaction rate constants for OP hydrolysis via hydroxide attack opposite the thiolate ligand. ....	29
Table 4. PVC pipe loops, bulk water physiological conditions. ....	31
Table 5. PVC pipe loops, biofilm conditions. ....	32
Table 6. ERDC-developed EPANET MSX physicochemical model simulations, showing the end state after 24 hours of a contamination event in two water distribution system layouts comparing hydrophilic contaminant distribution in water and on pipe walls. ....	39



## Preface

This study was conducted for Headquarters, U.S. Army Corps of Engineers, under Research, Development, Test, and Evaluation Program Element 21 2040 622784T41, “Military Facilities Engineering Technology;” Project 150162, “Molecular Modeling of Chem-Bio (CB) Contaminant Sorption / Desorption and Reactions in Chlorinated Water Systems.” The technical monitor was Dr. John Cullinane, Engineer Research and Development Center.

The work was performed by the Materials and Structures Branch (CF-M) of the Facilities Division (CF), U.S. Army Engineer Research and Development Center – Construction Engineering Research Laboratory (ERDC-CERL). At the time the work was conducted, Vicki L. Van Blaricum was Chief, CEERD-CF-M; L. Michael Golish was Chief, CEERD-CF; and Martin J. Savoie was Technical Director for Environmental Quality and Installations. The Deputy Director of ERDC-CERL was Dr. Kirankumar Topudurti and the Director was Dr. Ilker Adiguzel.

COL Kevin J. Wilson was the Commander and Executive Director of ERDC, and Dr. Jeffery P. Holland was the Director.

## Unit Conversion Factors

Multiply	By	To Obtain
inches	0.0254	meters

# 1 Introduction

## 1.1 Background

Army installations have a high density of critical facilities that are difficult to abandon in place, especially during force projection and deployment. Examples of such facilities include: Combatant Command (COCOM) Headquarters, Department of Defense (DoD) Command and Control Centers (C2), and all medical facilities. In the event of chemical-biological (CB) contamination of the water distribution system, such mission-critical facilities and their supporting installations would need protection. Accurate understanding of the fate and transport of contaminants is vital to ensuring adequate protection from intentional or accidental contamination events.

Previous U.S. Army Engineer Research and Development Center (ERDC) research<sup>1</sup> had formulated a physicochemical model that described how contaminants introduced to a potable water distribution system were capable of uptake (sorption) on pipe materials. This physicochemical model was validated using laboratory measurements:

$$\frac{P(t)}{C_0} = \beta(1 - e^{-t/\Gamma}) \quad \text{Equation 1}$$

where:

- $P(t)$  = concentration of contaminant on pipe material
- $C_0$  = initial concentration within the solution
- $\beta$  = fraction deposited on the wall at equilibrium
- $\Gamma$  = characteristic time constant

The two parameters,  $\beta$  and  $\Gamma$ , are measured experimentally for each combination of pipe material and contaminant. Below the saturation point of the contaminant in water, the parameter  $\beta$  is insensitive to concentration. This finding shows that the process is dominated by thermodynamic partition of the contaminant between water and pipe material, and that  $\beta$  can

---

<sup>1</sup> Direct-funded 6.2 research unit, "New Physicochemical Models of Fate and Transport of Contaminants in Potable Water Distribution Systems."

be measured in percentage uptake. This is a major update to physicochemical modeling of fate and transport of contaminants. Leaving these two parameters ( $\beta$  and  $\Gamma$ ) as unknowns that must be measured on a case-by-case basis for each pipe-wall-material/contaminant pair is not a totally satisfying result. In that scenario, conducting costly lab experiments on all likely contaminants that could interact with all common pipe materials ahead of an event is too expensive, and conducting the same types of experiments during or after an event is too slow to offer satisfactory remediation.

This pitfall was known at the time of ERDC's previous research so that contaminant data was also compared to simulant data in the hope that uptake could be predicted *ab initio* by using other commonly known properties of a prospective contaminant. The results of this line of research showed that chemical contaminant uptake is a function of the parameters given below.

- *Molecular weight*: Large molecules would have difficulty diffusing into the molecular matrix of the pipe wall material.
- *Hydrophobicity*: Hydrophilic materials are unlikely to have any affinity to pipe wall material.
- *Number of contact points*: Increasing the number of contact points between the contaminant and the pipe wall leads to greater uptake.

At the outset, the first two parameters were known to researchers. The experimental results obtained during this project guided us to the third parameter, the concept of "number of contact points." By obtaining a near match for both hydrophobicity and molecular weight, a high-quality simulant (simulant P) for an agent under study (agent V) could be selected.

Considering the prohibitive cost of performing laboratory studies on the behavior of all possible contaminants within a water distribution system, this project focused on the use of computational methods for the *ab initio* determination of rate constants.

This report demonstrates the inclusion of results from molecular modeling for the transport of contaminants by using the NAnoscale Molecular Dy-

namics program (NAMD)<sup>1</sup>, the influence of bacterial biofilms on spore viability in the presence in chlorinated water distribution systems, and computational chemistry predictions of the rate of hydrolysis of a specific contaminant into predictive software EPANet<sup>2</sup>. The inclusion of these initial values (Section 1.1) opens the way for further water-distribution simulation upgrades for better protection, remediation, and planning ahead of a contamination event.

## 1.2 Objectives

The objective of this work is to implement improvements to a simulation tool for planning courses of action (COA), passive protection, active protection, and decontamination. This is done by using experimentally validated molecular models for CB contaminant sorption/desorption kinetics using computational chemistry (CC) and NAMD, resulting in a pipe segment (PS) hydraulic model based on key kinetic parameters and variables.

## 1.3 Approach

The approach of this project can be broken down into three tasks that were concurrently executed:

- *Task 1:* For bulk reactions with chlorinated water species, the equations built into EPANet were adequate; however, there is no lookup mechanism to bring in the correct kinematic parameters into the simulation based on the contaminant selected. To accomplish this, we added routines to manage a library of such parameters. The use of this library should be transparent to the user who merely selects the contaminant of interest.
- *Task 2:* For pipe wall sorption / desorption, the equations built into EPANet were inadequate and we added them to the software. In addition, these equations require access to a library of kinematic parameters that is quite similar to that developed in task 1.

---

<sup>1</sup> NAMD is a parallel molecular dynamics code designed for high-performance simulation of large biomolecular systems. NAMD is distributed free of charge with source code ([www.ks.uiuc.edu/Research/namd/](http://www.ks.uiuc.edu/Research/namd/)).

<sup>2</sup> EPANet is an EPA-developed (Water Supply and Water Resources Division) software that models water distribution piping systems. It is a Windows-based program that performs extended-period simulation of the hydraulic and water quality behavior within pressurized pipe networks (<http://www.epa.gov/nrmrl/wswrd/dw/epanet.html>).

- *Task 3:* The kinematic parameters that populate the libraries were derived from a combination of molecular models (as outlined in Section 1.1 above) including: NAMD, Cosmotherm, and Gaussian. Also, careful characterization of biofilms was important from the standpoint of asking how much biofilms contribute to sorption and desorption and if they are suitable hosts for biological species of interest.

## **1.4 Scope**

The project's scope is a proof-of-concept for using computational chemistry to describe sorption-desorption of a family of contaminants grouped by molecular weight, and an initial modification of existing hydraulic model code (EPANet 2.0) to account for sorption-desorption.

## **1.5 Mode of technology transfer**

The technologies developed by this work will be transferred by imbedding the fate and transport kinetic parameters obtained into EPANet 2 MSX, the establishment of a Memorandum of Understanding (MOU) with the U.S. Environmental Protection Agency (USEPA) to continue joint research efforts pertaining to water security, and recommended changes to DoD guidelines.

## 2 Experimental Program

### 2.1 NAMD modeling

Conceptually, the parameters that need to be derived from NAMD and then plugged in to EPANet are easily summarized from the standpoint of statistical mechanics. We start by quoting the results required from the standpoint of thermodynamics and then show how the thermodynamic parameters are derived from NAMD simulations.

#### 2.1.1 Thermodynamic derivation of the uptake parameter $\beta$ for EPANet

First, we show that the uptake parameter ( $\beta$ ) is directly related to chemical potential. In the range of concentration above detectable limits and below saturation, the best approximation is a first-order interaction between the contaminant and the pipe surface that relaxes toward the equilibrium constant  $\beta$ . (One way of viewing this interaction from a conceptual standpoint is to compare it to the widely used octanol-water ratio. Another valid way to view our work is to think of this as a pipe-water ratio.) This relationship is reproduced again in Equation 2 as an uptake with one time constant and one equilibrium constant.

$$\frac{P(t)}{C_0} = \beta(1 - e^{-t/\Gamma})$$

Equation 2

where

$P(t)$  = concentration of contaminant on pipe material as of a function of time

$\beta$  = fraction deposited on the wall at equilibrium

$e$  = Euler's constant

$C_0$  = initial concentration within the solution

$\Gamma$  = characteristic time constant

The equilibrium of this equation is characterized by letting time go to infinity, yielding:

$$\frac{P(t)}{C_0} = \lim_{t \rightarrow \infty} \beta(1 - e^{-t/\Gamma}) = \beta$$

Equation 3

The chemical potential, denoted as  $E$  in Figure 1, is the amount of energy either gained or lost when a molecule of contaminant moves from the water onto the pipe. Chemical potential is, in essence, the binding energy of a contaminant to the pipe surface.

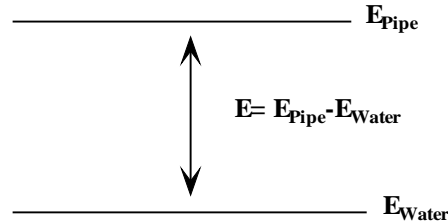


Figure 1. Graphic of chemical potential – the binding energy of a contaminant to the pipe surface.

Hence, the equilibrium state of the system is characterized by Equation 4.

$$\left. \frac{P(t)}{C(t)} \right|_{t \rightarrow \infty} = \frac{\beta}{1 - \beta} \quad \text{Equation 4}$$

where

$P(t)$  = concentration of contaminant on pipe material as a function of time

$C(t)$  = concentration of contaminant in the water as a function of time

$\beta$  = fraction deposited on the wall at equilibrium

This characterization means that the asymptotic uptake in the pipe ( $\beta$ ) is directly related to chemical potential. If the contaminant ends up almost entirely on the pipe or almost entirely in the water implies that  $|E| \gg kT$ .

Because NAMD is computationally efficient enough to measure the binding energy over a large number of molecules and binding events with the simulated pipe wall surface, we arrived at a valid estimation of the chemical potential by calculating the fraction of molecule bound to the wall and claiming that this calculation corresponds to the asymptotic uptake.

### 2.1.2 Derivation of the uptake time constant parameter $\Gamma$ for EPANet

Contaminant traveling as a slug will continually approach fresh, uncontaminated pipe. Thus, the rate of uptake can be estimated by looking at the



initial slope of the physiochemical uptake model (Equation 2). In other words, the derivative of the physicochemical uptake model is taken with respect to time and evaluating it at time,  $t=0$ , as shown in Equation 5.

$$Rate = \left[ \frac{\partial}{\partial t} \left( \beta (1 - e^{-t/\Gamma}) \right) \right]_{t=0} = \frac{\beta}{\Gamma} \quad \text{Equation 5}$$

## 2.2 Reaction rates with species in chlorinated water

This problem reduces to predicting two constants *ab initio*—the activation energy ( $E_a$ ) and the Arrhenius pre-factor ( $A$ ). The classical relation between two reactants is  $rate = r[A]^m[B]^n$  where  $[A]$  and  $[B]$  are the molar concentration of the two reactants,  $m$  and  $n$  are unknown constant exponents, and  $r = Ae^{-\frac{E_a}{kT}}$  with  $k$  being the Boltzmann constant and  $T$  being temperature.

When a reaction has rate constants that obey the Arrhenius equation, both  $A$  and  $E_a$  are read from a graph of  $\ln(r)$  vs.  $(1/T)$  at constant pressure, as shown in Equation 6.

$$E_a = -k \left( \frac{\partial \ln r}{\partial (1/T)} \right)_p \quad \text{Equation 6}$$

A graph of this function immediately yields  $E_a$  and  $A$ . This is used to validate predictions of both constants using software such as Gaussian.

*Ab initio* quantum chemical methods were used to investigate the hydrolysis of an organophosphate (OP) under alkaline conditions. The representative OP consisted of 42 atoms arranged in a complex branched structure. The structure of the OP was optimized *in vacuo* to find the minimum energy configuration using the 6-31+G(2d,2p) basis set (Figure 2). This basis set had been shown in previous studies (Wright et al. 2005) to yield results that were in good agreement with available experiments.

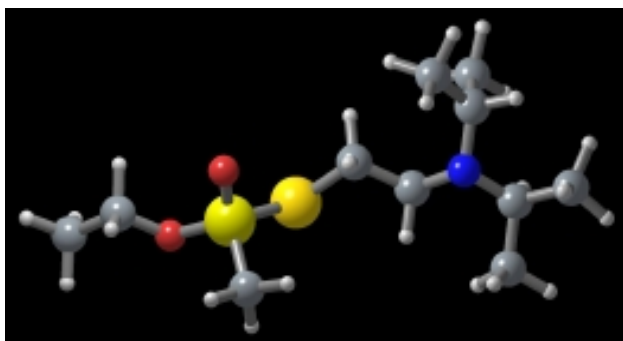


Figure 2. Optimized structure of an organophosphate.

Initial investigations into possible mechanisms for the alkaline hydrolysis of OP were carried out in the gas phase, to verify possible intermediate structures that had been obtained from the scientific literature. Using these structures as starting points, a detailed investigation of the behavior of the OP-hydroxyl interactions was undertaken using the Polarizable Continuum Model (PCM) to simulate liquid water implicitly as a continuum with a known dielectric constant. Transition State Theory (TST) was used to locate saddle points on the potential energy surfaces that correspond to transition states and other intermediates in the alkaline hydrolysis of OP. Pathways were carefully located and traced that linked transition states to reactants and products, to verify that the mechanism proposed was physically realizable. Activation energies for one of the possible hydrolysis pathways were obtained, and kinetic equations were solved to provide rate constants for the reactions.

## 2.3 Laboratory validation experiments

### 2.3.1 Prophos selection and analysis

Prophos was selected as a model contaminant because it is hydrophobic and represents a larger class of potential chemical contaminants of concern. In addition, it is similar in structure to the organophosphates whose uptake on surfaces has been studied by using molecular modeling, which allows comparisons between those results and the results of our laboratory experiments.

Prophos concentrations in solution were measured at the University of Illinois at Urbana-Champaign (UIUC) by using liquid chromatography/mass spectrometry (LC/MS) using a C-18 column. A two-component eluent mixture of (a) 95% water/5% acetonitrile and (b) 95% acetonitrile/5% water was run over a gradient shifting from 25%–70%

over the course of 20 min. The LC/MS response for a set of standards was linear in the range of interest, from 5 mg/L to 750 mg/L.

### 2.3.2 Reactor vessels

Four types of pipe reactor vessels were fabricated for these experiments from lengths of piping made from polyvinyl chloride (PVC), copper, and concrete-lined ductile iron (CLDI) as described below.

Sections of PVC pipe were cut to 6 in. in length. A standard PVC primer was applied to one end of the pipe where the vessel would be capped. PVC cement was then applied over the primer. Stock PVC caps were attached to the pipe segments. Care was taken to ensure that no primer or cement migrated into the reactor chamber during assembly.

The copper reactor vessels were also prepared using 6-in. lengths of pipe. Stock copper end caps were attached using standard flux and lead-free solder. Care was taken to ensure that no flux or solder migrated into the reactor chamber when the cap was attached. Both PVC and copper reactor vessels were set in tip-resistant PVC cups as shown in Figure 3.



Figure 3. Reactor vessel (PVC) placed in tip-resistant PVC cup.

Two different types of CLDI reactor vessels were made. The first vessel was coated with asphaltic sealer, which is the current standard for coating new pipe materials of this type. The second vessel was unsealed CLDI, to represent the large inventory of pipe currently in place in older water distribution systems. Both vessels were cut to approximately 6-in. length. The ex-

posed ends of the pipe segments were passivated with marine-grade epoxy, and one end was attached to a standard glass Petri dish. The laboratory-grade glass in the Petri dish was tested and shown not to interact significantly with the substances of interest. Care was taken during the assembly to prevent the epoxy from migrating into the reactor chamber. The Petri dish was of large enough diameter that no additional tip-resistant cup was required for stability in the laboratory. Figure 4 shows the three PS types as assembled.



Figure 4. Three pipe reactor vessels as assembled.

In order to condition the pipe materials, deionized water was placed in the vessels and covered with parafilm. The water was changed every 1–2 days for 1 week. The PS were then allowed to dry overnight.

### 2.3.3 Experimental set-up

The prophos uptake experiments were run at three different concentrations: 750 mg/L, 250 mg/L, and 125 mg/L. Four replicate set-ups of each pipe material and concentration combination were run.

The prophos solutions were added to the pipe segments, after which the initial set of samples was collected by removing 1 mL of solution and transferring it to a vial for later analysis. The vessels were then covered in parafilm to inhibit contamination and evaporation between sampling times. Subsequent sampling was performed periodically over the next 2 to 12 days, with four replicate set-ups of each pipe material and concentration combination.

## 2.4 Biofilm studies

Bacterial biofilms are dynamic structures that are composed primarily of polysaccharides, microbial cells, and water. Planktonic bacteria are known to readily incorporate into biofilms, which can conversely increase their resistance to free chlorine up to 3000-fold. The two-fold purpose of this task was to: (1) characterize a biofilm in relation to varying free available chlorine in a simulated water distribution system; and (2) investigate *Bacillus globigii* spore uptake within established biofilms.

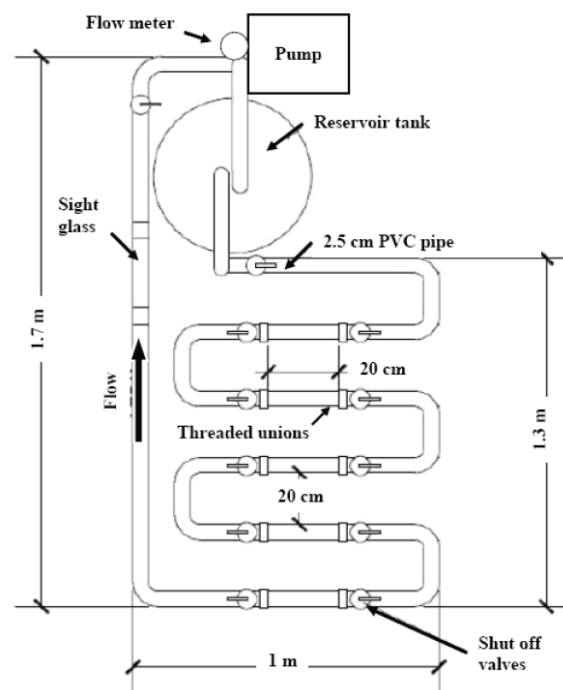
### 2.4.1 *Bacillus globigii* preparation and enumeration

Dehydrated, non-weaponized *Bacillus globigii* spores were obtained from Dugway Proving Ground (Dugway, UT). Spore viability was analyzed by 10X serial dilutions over seven orders of magnitude, followed by heat-shocking at 80 °C for 10 min, and direct plating 100 µL of each dilution series onto tryptic soy agar (TSA; Fluka, Milwaukee, WI). All dilutions were plated in triplicate and incubated for 48 hr at 35 °C. Orange colony forming units (CFUs) were enumerated, and plates that yielded 50–200 CFUs were used in conjunction with the dilution factors to calculate the spore concentration of the undiluted sample.

### 2.4.2 Experimental drinking water system

Three separate PVC loop systems were operated at different free chlorine concentrations — 0.0, 0.5, and 1.0 mg/L as Cl<sub>2</sub>. Each pipe loop was fabricated out of schedule 40 PVC pipe (2.5-cm diameter) with a total loop length of 10 m. The total volumetric capacity of the pipe loop system, including the bulk water reservoir, was 17 L. Each loop contained five removable 20-cm pipe segments for sampling of biofilm (Figure 5). Flow was controlled by a magnetic drive centrifugal pump to achieve an average velocity of 30 cm/sec, measured using an inline flow meter. Clear PVC sight glasses measuring 30-cm in length were installed in front of each pump head to visually observe biofilm formation on the pipe surface. 20-L carboy reservoirs were covered with black plastic to minimize phototrophic growth. Each loop system was operated at ambient room temperature, approximately 25 °C. Flow rate, temperature, pH, and free chlorine in each pipe loop were monitored daily.

(A)



(B)

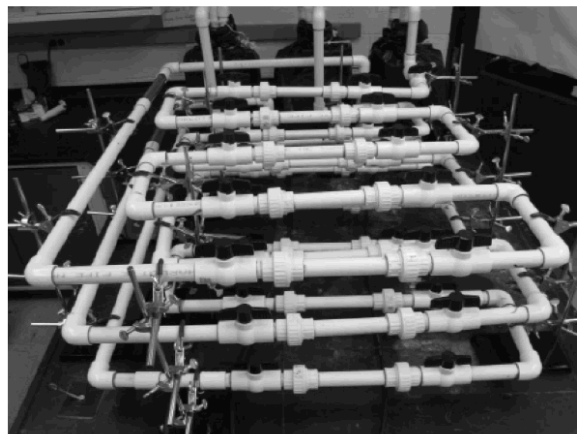


Figure 5. Simulated PVC water distribution system: (A) Illustration of pipe loop system constructed with standard 2.5-cm PVC pipe and fittings. Three separate systems were constructed, each having a total length of 10 m, bulk phase volume of 17 L, operation temperature of approximately 25 °C, and a flow rate of 30 cm/sec; (B) The loop systems in operation—each was allowed to acclimate for 63 days as one unit then individually poised at 0.0, 0.5, and 1.0 mg/L free chlorine with sodium hypochlorite 3 days prior to the addition of *B. globigii* spores.

Prior to experiments, pipe loops were flushed with tap water for a two-week period to remove residual organics that were present from the pipe manufacturing process and the joint cement. After the initial flushing, each loop was completely drained and filled with dechlorinated tap water. Chlorine was removed by the addition of sodium thiosulfate to a final concentration of 8 mg/L. All three loop system reservoirs were temporarily connected to each other with a diverter valve, to allow water to flow freely between each system for promoting homogeneous biomass formation. Visual inspections of biofilm formation were made periodically through the sight glasses and optical densities at 600 nm were taken from the re-circulating tanks as a measurement of planktonic growth. Synthetic tap water, periodically amended with 50 mg humic acid, was used to stimulate biofilm growth.

After an additional 28 days of continual operation, the pipe loops were drained and flushed with dechlorinated tap water to remove residual nutrients and excess planktonic bacteria. Each pipe loop was then isolated, and two of the three loops were amended with a 10% sodium hypochlorite solution to final free chlorine concentrations of 0.5 and 1.0 mg/L. After three additional days of circulation, each loop system was inoculated with *B. globigii* to a final viable density of approximately  $1.8 \times 10^4$  CFUs/mL.

#### **2.4.3 Bulk water and biofilm sampling**

Bulk water and biofilm samples were taken from each pipe loop after 10 min and then 3, 7, 14, and 21 days of circulation. Liquid samples were collected from each reservoir tank using sterile 50-mL pipettes. Biofilm samples were obtained at predetermined time intervals by removing one sampling segment per loop in a sequential order. Segments were replaced with sterile PVC segments of the same dimension. The removed pipe segments were gently rinsed with sterile ultra-pure water to remove residual planktonic bacteria. Three 2-cm sections were cut from the center of each pipe segment using a PVC pipe-cutter sterilized with 90% ethanol. Biofilms were harvested by scraping. Bulk water samples, biofilm scrapings, and remaining sample port segments were immediately preserved at  $-20\text{ }^{\circ}\text{C}$  until further analysis.

#### **2.4.4 Bacterial enumerations**

Heterotrophic plate counts (HPCs) and *B. globigii* viability assays were conducted with both bulk water and biofilm scrapings by using plating

methods described in Section 2.3.1 with plates containing plate count agar (Fluka) and TSA, respectively. Plates were allowed to incubate for 48 hr at 35 °C, and CFUs were counted on plates within a given dilution series having 50–200 colonies. Levels of inactivation were evaluated by plotting the normalized fraction of survivors ( $N_t/N_0$ ) against exposure time (days). Values were expressed as the total number of heterotrophs or spores in each pipe loop system.

#### **2.4.5 Water quality and biofilm characterization**

Bulk water-free chlorine concentrations were monitored using U.S. Environmental Protection Agency (USEPA)-approved *N,N*-diethyl-*p*-phenylenediamine (DPD) photometric method (American Public Health Association 1995) using a DR/2000 spectrophotometer (HACH, Loveland, CO). Total polysaccharide content of the biofilm scrapings was determined with a modified colorimetric phenol-sulfuric acid method (Dubois et al. 1956). Total extra-cellular enzyme content was evaluated using a Coomassie Plus Better Bradford Protein Assay Kit (Pierce Distribution, Rockford, IL) according to the manufactures micro test tube protocol. Free nucleic acids (ssDNA, dsDNA, and RNA) present were quantified using a Quant-iT™ ssDNA Assay Kit (Invitrogen, Eugene, OR) according to the manufactures protocol. Bulk water and biofilm data were reported as the means  $\pm$  standard deviation (SD) where  $n = 3$ .

#### **2.4.6 Microscopy**

Nonviable spores within biofilms were qualitatively assessed by light microscopy using a Nikon Eclipse E400 light microscope (Melville, NY) equipped with an Insight digital camera and Spot imaging software (Diagnostic Instruments, Inc., Sterling Heights, MI). Spores were differentially stained using a malachite green method as described by Schaeffer and Fulton (1993).



## 3 Results and Discussion

### 3.1 Atomic resolution modeling – two phases

Our efforts to describe the transport of chemicals and biomolecules through waterworks had two phases.

#### 3.1.1 Phase 1: Atomic-scale features and molecule interaction with surfaces

The first effort was to understand how atomic-scale features of model pipe surfaces affect the interaction of the molecules with the surfaces, and therefore, determine the binding and unbinding rates of the molecules at a given concentration. This phase required all-atom molecular dynamics simulation using NAMD. Below we describe how the development of all-atom models for the simulation of pipe surfaces and contaminant molecules, as well as the results of methods used to characterize their interaction. This characterization was performed through the creation of atomic-resolution, three-dimension (3-D) potential of mean force (PMF) maps, which subsume electrical, van der Waals, and water-mediated interactions. In addition to allowing the effect atomic-scale features on molecule–surface binding to be determined, these maps also permitted development of the multi-scale models used in the second phase.

#### 3.1.2 Phase 2: Transport of molecules near surfaces

In the second phase, we investigated explicit transport of molecules near surfaces through atomic-scale simulation. This was done first through all-atom molecular dynamics (MD) simulation using NAMD; however, the computational expense of all-atom models limits its use to nanoscale systems and short timescales. Thus, we have developed multi-scale models using PMF maps derived from all-atom MD simulations that are much more computationally efficient than all-atom MD simulations yet lose little of the atomic-scale detail required to describe realistic molecule–surface interaction. These multi-scale models extend our simulations to long timescales and large spatial scales, in addition to providing the ability to fully explore effects like concentration dependence on solute binding. We expect the results and the methodologies developed from this work will be of interest not only for those modeling solute transport through public waterworks, but also in the field of nanofluidics, where the prominence of so-

lute–device surface interactions can lead to unexpected behavior and even render the device useless.

### 3.1.3 Nanoscale models of pipe surfaces

To investigate interactions of chemicals and biomolecules with pipe surfaces at atomic resolution, we first needed a description of the pipe surface at the same level of detail. To this end, we created four nanoscale models of pipe surfaces (Figure 6).

The first model represents the simplest case: An infinitely smooth, frictionless surface, which acts as a hard boundary to reflect molecules (Figure 6A). This surface did not consist of atoms; instead this surface was modeled by applying a smooth potential to all the atoms in the simulation. We have implemented this in NAMD, the molecular dynamics package developed at UIUC through the grid-steered molecular dynamics (G-SMD) method developed by our research group.

To model the affects of surface hydrophobicity and atomic-scale roughness on solute adsorption, we created three all-atom model pipe surfaces composed of silica ( $\text{SiO}_2$ ). To produce the silica membranes used in our research, we created a  $2.5 \times 2.5 \times 3.5 \text{ nm}^3$  block of crystalline silica containing 500 silicon and 1000 oxygen atoms by replicating a silica unit cell. The model membrane was annealed through a regimen of simulations, where it was first simulated at high temperatures (7000 K) and gradually cooled to room temperature. Coordinates of the silica membrane were chosen from three points in this regimen to produce three distinct surfaces, varying from smooth (Figure 6A) and hydrophobic (Figure 6B), to a surface of intermediate properties (Figure 6C), to rough and hydrophilic (Figure 6D).

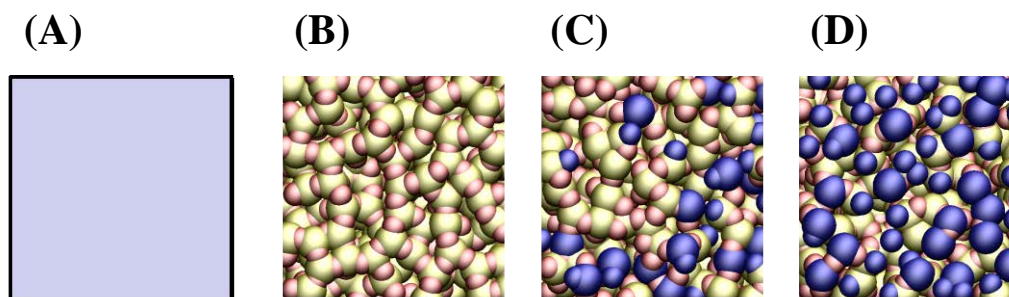


Figure 6. Nanoscale models of pipe surfaces: (A) frictionless, (B) hydrophilic, (C) intermediate, and (D) hydrophobic

### 3.1.4 All-atom model of DMMP

To study the transport and sorption/desorption of organophosphonates through model nanochannels, we chose dimethyl-methylphosphonate (DMMP). However, at the time of our study, there were no all-atom parameters available for DMMP that were compatible with the Chemistry at HARvard Macromolecular Mechanics<sup>1</sup> (CHARMM) force field, upon which our models for proteins and silica rely. Therefore, we adapted the united-atom DMMP parameters developed by Vishnyakov and Neimark (2004) for use with the CHARMM force field. The modified parameters were evaluated through numerous MD simulations at three different concentrations, and the dynamics of the modified DMMP model were found to be in agreement with the united-atom model.

### 3.1.5 Characterization of molecule-surface interactions

To characterize the surfaces and determine the connection between atomic-scale surface roughness and solute binding, we calculated the 3-D PMF between the DMMP molecule and each surface by using umbrella sampling MD simulations. A diagram describing this calculation is shown in Figure 7.

The PMF at a given position represents the potential energy of the particle corresponding to the average force exerted on the molecule at that position. In agreement with our MD flow simulations, we found that silica surface B is the most attractive, followed by surfaces C, D, and A, with the latter being the frictionless surface. Silica surface B shows a strong correspondence between the atomic-scale topography and DMMP binding strength. The similarity in topography between silica surface B and C leads us to conclude that in addition to the topography, there are other surface features (e.g., local surface charge density) that play a role in binding.

---

<sup>1</sup> CHARMM is a versatile and widely used molecular simulation program with broad application to many-particle systems.

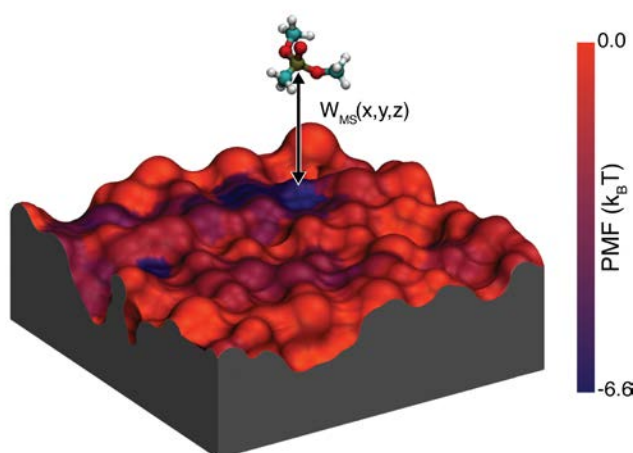


Figure 7. PMF calculations. The DMMP-surface PMF ( $W_{MS}$ ) was calculated as a function of the position of the DMMP over each surface. The silica surface is colored by the value of the PMF at that position of the surface. The DMMP is most attracted to the regions with the lowest PMF (shown in purple).

### 3.1.6 Model nanochannels

All-atom molecular dynamics simulations are limited to length scales of tens of nanometers. Furthermore, to increase computational efficiency and accuracy, we imposed periodic boundary conditions. Thus for our studies of the interactions between chemicals or biomolecules and pipe surfaces, we simulated solutions of chemicals or biomolecules flowing in nanochannels. While there is a disparity between the height of a nanochannel and the interior of a pipe, we have shown that the length-scale of the molecule–surface interaction, using PMF, is short enough that the majority of the solution in the nanochannel is in the bulk phase — justifying the use of our model.

We created atomic-scale model nanochannels (Figure 8) from the frictionless and silica membranes by imposing periodic boundary conditions that defined the spacing between the nanochannel walls (the channel's height) and made the channel effectively infinitely long and wide. Depending on the study, the volume inside the nanochannel was filled with a solution of pure water, water and chemicals, or water and protein. Typical dimensions of the nanochannels in our study were  $5.5 \times 10 \times 10 \text{ nm}^3$ .

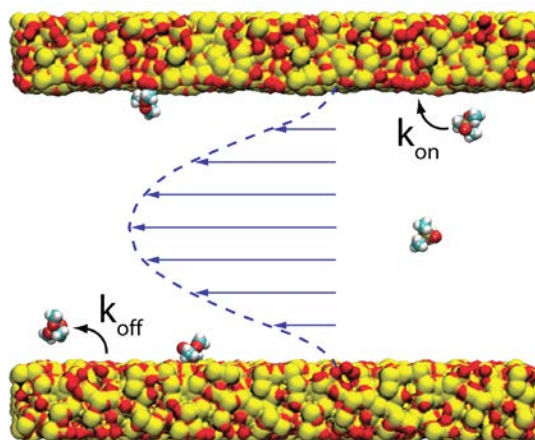


Figure 8. Diagram of solute transport through a silica nanochannel. The average water profile calculated from the all-atom MD simulations is shown in blue. Solutes are transported by the flow of water through the channel and spontaneously bind and unbind on the channel surface. The binding constants ( $k_{off}$  and  $k_{on}$ ) calculated from all-atom MD simulations were used as inputs to EPANet.

### 3.1.7 NAMD simulations of solute transport

To induce water flow through a nanochannel, a constant pressure difference was created by applying a lateral force to all the water molecules in the system, which results in a pressure difference across the system (Equation 7).

$$\Delta P = NF/A \quad \text{Equation 7}$$

where:

$P$  = pressure

$N$  = atoms

$F$  = lateral force

$A$  = area perpendicular to the applied force

We simulated the flow of water through silica nanochannel B at five different pressure gradients. From these simulations, we determined that the mass flux of water through the nanochannel will scale linearly, with the applied pressure gradient within the entire range of pressure gradients tested (spanning three orders of magnitude). Furthermore, the simulated water profiles were found to be accurately described as a Poiseuille flow through an infinite channel. However, some deviations from the theoreti-

cal predictions were observed within 0.5 nm of surface of the channel, where the breakdown of the continuum description could be expected.

For the remaining nanochannels, we repeated the simulations at two pressure gradients and confirmed the same behavior. From these simulations, it was seen that the transport properties of the silica channels were very similar, meaning that surface properties play a limited role in water transport through the nanochannel. In contrast to the silica surfaces, the frictionless surface has flat water velocity profile (a “plug” flow), due to the “slip” boundary condition at the surface.

When the same simulations were performed with the water replaced by a solution of DMMP, we found similar behavior, but with an increased viscosity of the fluid that caused a reduction in the mass flux. The addition of DMMP also reduced the water velocity near the surface, as DMMP adsorbed on the channel surfaces. The rough, hydrophobic surface (Figure 6D) bound almost all of the DMMP in solution; the intermediate surface (Figure 6C) bound a majority of the DMMP; and the smooth, hydrophilic surface (Figure 6B) bound less than half the DMMP in solution. In contrast, the frictionless surface (Figure 6A) bound a quarter of DMMP in solution. From these simulations, we find that the DMMP molecules are attracted to hydrophobic surfaces, yet atomic-scale surface roughness also plays a large role in solute binding.

### **3.1.8 Biomolecular transport in nanochannels**

To understand the process of protein sorption on pipe and nanofluidic device surfaces, we performed the all-atom MD simulations of protein transport with a pressure-driven flow through a nanochannel. With these simulations, we characterized (with atomic resolution) the adsorption of a model protein to a silica surface. Although the simulated adsorption of the protein was found to be nonspecific, it had a dramatic effect on the rate of the protein transport.

To determine the relative strength of the protein–silica interactions in different adsorbed states, we simulated flow-induced desorption of the proteins from the silica surface. Our analysis of the protein conformations in the adsorbed states did not reveal any simple dependence of the adsorption strength on the size and composition of the protein–silica contact, suggesting that the heterogeneity of the silica surface may be an important factor. In addition, we outlined a general computational method for char-

acterization of interactions between proteins and heterogeneous inorganic surfaces and performed a proof-of-principle demonstration of the method using the frictionless surface.

### **3.1.9 Continuum transport model for solutes in nanochannels**

All-atom MD simulations of solute binding in nanochannels are computationally demanding, limiting the variations in simulation parameters that can be explored. In our research, we sought a computational method by which we can model solute binding with atomic precision, yet have less computational costs than an all-atom MD simulation, so we can fully explore all the available parameters cheaply and quickly.

To this end, we created a continuum transport model for solutes in a nanochannel. In this model, we solve the Smoluchowski equation, which is essentially a modified diffusion equation, parameterized with the calculated diffusion constant of the solute and the calculated PMF of solute near each surface. The Smoluchowski model allows us to predict both the flux of DMMP molecules onto the channel membrane in the initial phase of the simulations, as well as the fraction of molecules that are bound to the surface in the steady state. For the frictionless surface, the Smoluchowski model properly predicts both the transient and steady-state behavior of the MD simulations. However, the model breaks down for the silica surfaces, because the silica surface PMF varies largely over the surface and the continuum model has no particle exclusion so that crevices in the silica surface accumulate too many particles.

### **3.1.10 Brownian dynamics transport model for solutes in nanochannels**

In order to overcome the obstacles we faced in the Smoluchowski model, we have written a Brownian dynamics (BD) simulator. When parameterized with the calculated diffusion constant of the solute, the PMF for the solute near the surface, and the calculated PMF between two solutes, we can perform BD simulations that recreate the results of our all-atom MD simulation. In effect, we can simulate the transport of solutes through nanofluidic devices with atomic resolution, yet with a fraction of the computational cost of an MD simulation. Additionally, we can now explore the dependence of binding on concentration and initial conditions, which were too computationally demanding for MD. Reference detail for BD appears in Figure 9 and Figure 10 (Carr et al. 2011a, 2011b).

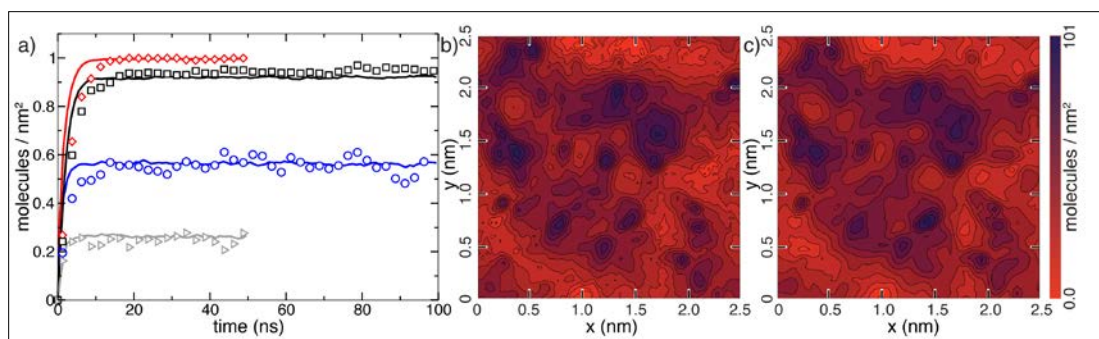


Figure 9. Comparison of Brownian dynamics (BD) with all-atom molecular dynamics. (a) The concentration of DMMP bound to the surface of each nanochannel system is a function of time, wherein MD results for Surfaces A, B, C, and D (Figure 6) are shown as gray triangles, red diamonds, black squares, and blue circles, respectively, with averages over 25 unique BD trajectories for each nanochannel shown with lines of corresponding colors; (b) DMMP bound to Surface D as a function of position—MD results are on the left, while BD results are on the right. The BD captures the surface characteristics with atomic resolution detail.

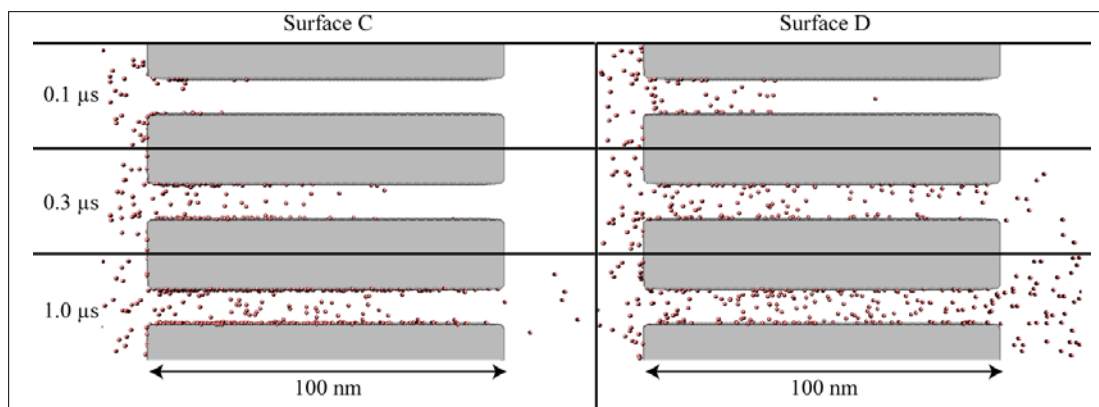


Figure 10. Atomic resolution BD simulation of DMMP advection through a 100 nm-long nanochannel for Surfaces C and D of Figure 6. A 10-mM concentration of DMMP is maintained on the left end of the channel, while the right end has an absorbing boundary. DMMP binds more strongly to the channel lined with Surface C than with Surface D; therefore, more time is required for DMMP to reach the end of the channel in the first case than for the second case, despite the identical water flow profiles.

### 3.2 Laboratory validation experiments

We now show that previous research that attempted to predict sorption of contaminant onto pipe material requires understanding the number of contact points between the contaminant molecule and the pipe wall. The following hypothesis will be shown to be inadequate. Suppose that chemical agent uptake is a function of the following two parameters:



- **Molecular Weight:** This makes intuitive sense in that sufficiently large molecules would have difficulty diffusing into the molecular matrix of the pipe wall material.
- **Hydrophobicity:** This also makes some intuitive sense in that hydrophilic materials were unlikely to have any affinity to pipe wall material. As a quantitative measure of hydrophobicity, we selected the water-octanol partition coefficient.

Both of these measures allowed us to select a high-quality simulant (Simulant P) for an agent under study (Agent V). Representative results from the current project are summarized in Table 1.

**Table 1. Representative results for high-quality simulant and studied agent.**

	Agent V	Simulant P	Exp. Error
Molecular Weight	267	242	
Water octanol partition coefficient	123	140	
β w/ CLDI w/ sealer	45%	100%	5%
T w/ CLDI w/ sealer	43 hours	77 hours	2 hours
β w/ cPVC pipe	42%	4.60%	5%
T w/ cPVC pipe	104 hours	107 hours	2 hours

Here we see that the prediction of matching molecular weight and hydrophobicity works reasonably well. The disagreement of measurements between Agent V and Simulant P are easily explained by the sensitivity of partition coefficient to small changes in chemical potential. However, the yellow line in Table 1 shows that some difference between the agent and its simulant has escaped our attention. The factor of ten separating the two measurements is too large to ignore.

We next included a conjecture that since chlorinated polyvinyl chloride (cPVC) is quite hydrophobic as a material, there would be increased van der Waals forces between the agent molecule and the pipe-wall surface. If Agent V is making contact with the wall at two points, where Simulant P makes contact at only one, we would expect that Agent V would undergo much more aggressive uptake and the increase in chemical potential would be somewhere in the range of 1–3 kcal/mol.

We then calculated the magnitude change in chemical potential and determined if the value is within the predicted range. The experimental results already gave percentage-uptake of contaminant on the pipe material;

therefore, we can calculate the partition coefficient showing the relative affinity of the agent for water versus pipe material (Equation 8).

$$\frac{C_{PIPE}}{C_{WATER}} = \frac{\beta}{1 - \beta} \quad \text{Equation 8}$$

where:

$C$  = concentration of the agent in the subscripted material

$\beta$  = asymptotic fractional uptake of material in the pipe

$E$  = the chemical potential

$k$  = Boltzmann's constant

$T$  = ambient temperature of the experiment

Thus the change in chemical potential when we substitute the simulant for the agent is represented by Equation 9.

$$\Delta E = -kT \ln \left[ \frac{(\beta_{Simulant})}{(\beta_{Agent})} \right] \quad \text{Equation 9}$$

Substituting appropriate numbers into this equation we get  $\Delta E = 1.31$  kcal per mole. This is easily within the range predicted by the “one versus two contact point” conjecture outlined above. Subsequent chemical modeling obtained by Ginsberg (ERDC) and Hurley (ARL) revealed that this conjecture is quite reasonable, as shown in Figure 11 and Figure 12 (Ginsberg et al. 2008).

In Figure 11 and Figure 12, the molecules of Simulant P and Agent V are depicted in 3-D form as ball-and-stick diagrams surrounded by translucent electron clouds. The coloring of the electron cloud shows the polarity of the electron cloud as a function of position. Intense red or intense blue depict those areas where the molecule has a high polarity or would be hydrophilic. The green areas are where the molecule is nonpolar or hydrophobic.

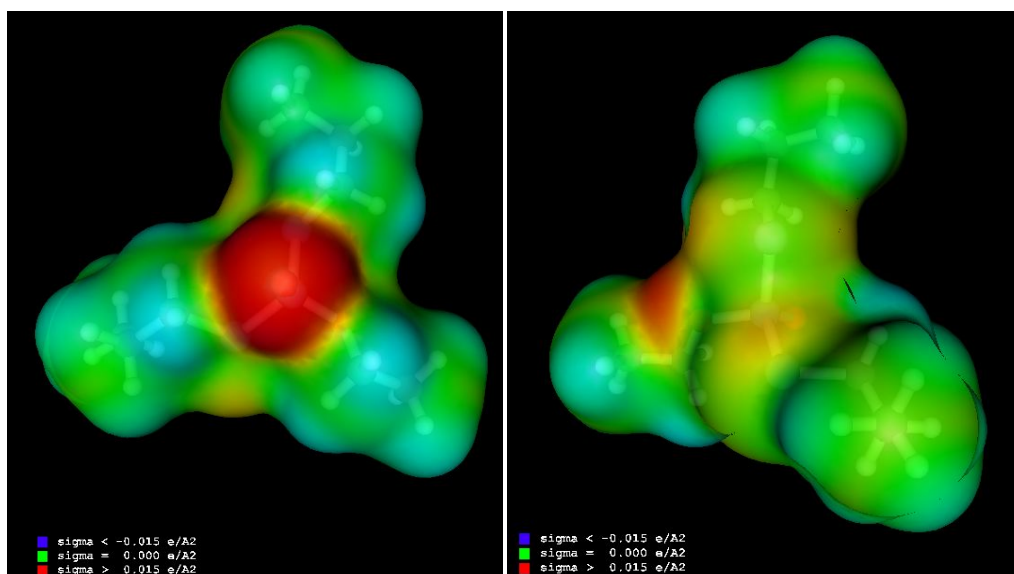


Figure 11. The 3-D depiction of Simulant P. View at left shows the molecule from the double-bonded oxygen side (easily seen by the intense red spot), and the right view is the obverse side. Polar regions are shown in red and blue; nonpolar regions are shown in green. The molecule is pinwheel shaped and is likely to have a single contact point with a nonpolar surface.

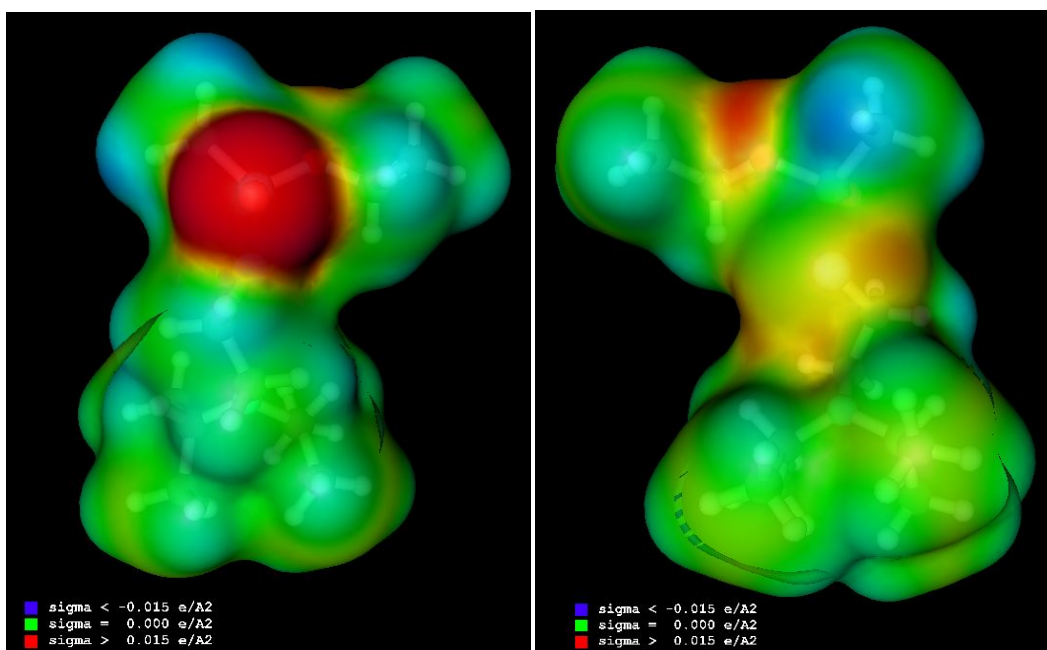


Figure 12. The 3-D depiction of Agent V. Left view shows the molecule from the double-bonded oxygen side of the molecule (easily seen in the intense red spot); the view at right is the obverse side. Polar regions are shown in red and blue; nonpolar regions are shown in green. Notice that the nonpolar region at the bottom of the molecule is likely to have two contact points.

Both molecules have a double-bonded oxygen site which results in a highly polar red spot. The molecule is very unlikely to make initial contact with the pipe wall at this point. The Simulant P is a largely pinwheel-shaped molecule and quite unlikely to make contact with the pipe wall at more than one point. However, Agent V does have a large region opposite the polar oxygen double bond that is quite likely to make contact with the pipe wall at two points.

### 3.3 Hydrolysis reaction rates and activation energy

In alkaline solutions, the hydrolysis of OP can occur via attack opposite the ethoxide or thiolate ligand. For the work described in this report, calculations were carried out for hydroxide attack opposite the thiolate ligand. As shown in Figure 13, the hydrolysis proceeds step-wise.

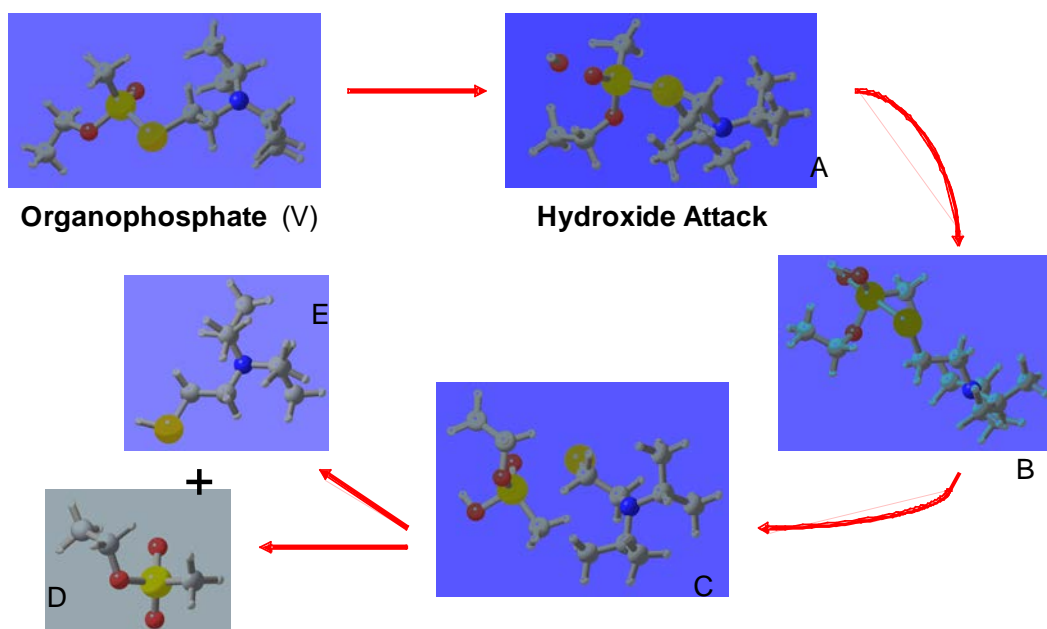


Figure 13. Clockwise from upper left: the step-wise hydrolysis of an organophosphonate via attack opposite the thiolate ligand. (The representative colors are yellow = phosphorus, dark yellow = sulfur; red = oxygen, blue = nitrogen, grey = carbon, and white = hydrogen.)

A hydroxide molecule must first align itself with the phosphonate center in the OP molecule. It subsequently binds to the phosphorus atom, destabilizing the phosphorus-sulfur (P-S) bond and resulting in bond cleavage. The rate-determining-step (i.e., the slowest of the reactions) for the proposed mechanisms is the initial alignment of the hydroxyl radical with the phosphonate center of the OP molecule. The transition of OP to a bound state with hydroxide through the aligned intermediate A requires activa-

tion energy of 21.08 kcal/mol. Subsequent steps in the hydrolysis pathway are energetically favored (Figure 14).

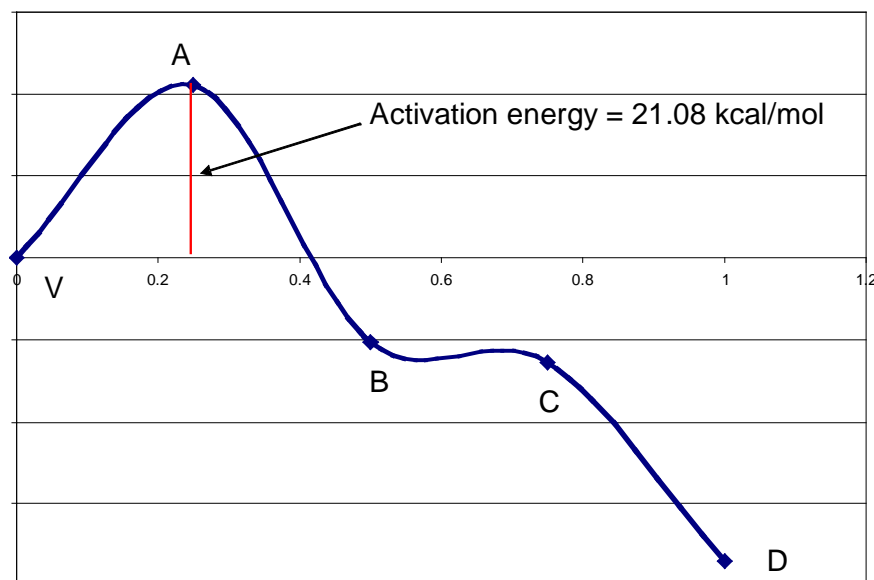


Figure 14. Changes in the energy of intermediate states in the hydrolysis pathway.

Reaction rate constants were also calculated for each step of the hydrolysis reaction shown in Figure 14. The values were calculated by using TST according to Equation 10.

$$r_{ij}(T) = \left( \frac{kT}{h} \right) e^{\frac{-G_{TS}(ij)}{RT}}$$

Equation 10

where:

- $r_{ij}(T)$  = rate constant of the transition  $i$  to  $j$
- $k$  = Boltzmann constant
- $h$  = Planck's constant
- $R$  = gas constant
- $T$  = temperature, 298.15 K for these calculations

The calculated rate constants are summarized in Table 2. As expected, the rate constant for the alignment of a hydroxide molecule with the OP is significantly slower (by several orders of magnitude) than the other reactions.

Table 2. Reaction rate constants for OP hydrolysis via hydroxide attack opposite the thiolate ligand.

Reaction	Rate Constant [sec <sup>-1</sup> ]
V → A	2.2 x 10 <sup>-13</sup>
A → B	7.7 x 10 <sup>35</sup>
B → C	3.2 x 10 <sup>14</sup>
C → D	4.3 x 10 <sup>28</sup>

Calculations of hydrolysis activation energy and reaction rate constants under varying pH and temperatures were performed for comparison, based on previously reported laboratory data (Morrissey et al. 2009). Half-lives ( $t_{1/2}$ ) at pH 8 and 14 were obtained from the report and used to calculate rate constants according to Equation 11, assuming a first-order reaction.

$$r = \frac{\ln 2}{t_{1/2}} \quad \text{Equation 11}$$

Reaction rate constants were also calculated from values for the time required to achieve 99.9% hydrolysis at different temperatures according to Equation 12.

$$C = C_0 e^{-rt} \quad \text{Equation 12}$$

where:

C = the concentration at time t

C<sub>0</sub> = the initial concentration

Table 3 lists the first-order reaction rate constants obtained for OP hydrolysis from the above calculations.

Table 3. Reaction rate constants for OP hydrolysis via hydroxide attack opposite the thiolate ligand.

pH	Temperature [K]	Rate Constant [sec <sup>-1</sup> ]
8*	298	1.1 x 10 <sup>-6</sup>
14*	298	9.6 x 10 <sup>-3</sup>
8^	278	6.6 x 10 <sup>-8</sup>
8^	288	2.7 x 10 <sup>-7</sup>
8^	298	1.1 x 10 <sup>-6</sup>

\* Data taken from Morrissey et al. 1999a; ^ Data taken from Morrissey et al. 1999b

These reaction rate constants are considerably more rapid than those obtained from the computational predictions for the rate limiting step. However, two key points must be made. Firstly, the calculations for the modeling focused only on one hydroxide attack site. Hydroxide attack may also align and subsequently bind to the phosphorus opposite the ethoxide ligand. Additionally, the modeling calculations were in essentially infinitely basic solution. As demonstrated by the laboratory data, the pH (and thus the availability of hydroxide) plays a significant role in reaction rate constants.

In summary, a direct comparison of reaction rate constants is difficult due to the variations in conditions assumed for the calculations. However, activation energy for hydrolysis is less dependent on the conditions of the system. For the laboratory data, activation energy can be calculated from reaction rate constants determined at different temperatures as shown by Equation 13 and Equation 14.

$$r = Ae^{-\frac{E_a}{RT}}$$

Equation 13

$$\therefore \ln r = -\frac{E_a}{RT} + \ln A$$

Equation 14

where:

$r$  = amount of reagent present

$E_a$  = activation energy

$R$  = Boltzman's constant

$T$  = time

$A$  = Constant

So, a plot of  $\ln r$  vs.  $1/T$  gives a slope of  $-\frac{E_a}{R}$ .

Multiplying by  $-R$  yields the activation energy. For the hydrolysis of an organophosphate data we have available, the activation energy is 23.06 kcal/mol, which is within 10% of the value obtained from the computer simulations.

### 3.4 Biofilm characterization and spore fate

The biofilm environments were characterized by daily measuring of free chlorine concentration, temperature, and pH during the 21-day period. Measured values from the days on which bacterial enumerations took place are reported in Table 4. Free chlorine values remained relatively stable throughout the study. Concentrations in the 0.5 mg/L and the 1.0 mg/L amended loops varied throughout the study by 0.1/L and 0.3 mg/L, respectively. No free chlorine was detected in the untreated pipe loop until after the addition of sodium hypochlorite on Day 14. Temperatures fluctuated less than 0.5 °C between each of the three pipe loops on a given day. Slight variations in pH were observed among the pipe loops; however, readings remain well within the range of a typical potable water distribution system (World Health Organization 2007). Due to the tremendous physiochemical tolerances associated with *Bacillus* spores (Nicholson et al. 2000), the slight variability in these physiochemical parameters were not believed to have a significant effect on *B. globigii* resistance within any given pipe loop over the course of the study. Turbidity was monitored prior to the start of the study as an indicator of biological activity. Each of the pipe loop systems increased in absorbance from 0.01 to 0.03 after three weeks of circulation in the presence of humic acid. Consistency of these ratios indicated that each pipe loop contained similar levels of biological activity. This consistency was confirmed by enumerating the bulk water heterotrophs, which revealed that each system contained approximately  $3.4 \times 10^5$  CFU/mL prior to flushing the system. The untreated pipe loop harbored  $1.4 \times 10^4$  CFU/cm<sup>2</sup> at the start of the study, which was indicative of a mature water distribution system (Schwartz et al. 2003). These data demonstrated that the conditions in each of the pipe loops were similar at the onset of the study and that each remained stable throughout the 21-day circulation period.



Table 4. PVC pipe loops, bulk water physiological conditions.

	Time (days) <sup>b</sup>				
	0	3	7	14	21
<b>0.0 mg/L free chlorine<sup>a</sup></b>					
Free Cl <sup>-</sup> (mg/L)	0.0	0.0	0.0	0.0	0.9
Temperature (°C)	23.3	25.4	22.8	26.4	23.2
pH	7.5	7.2	7.4	7.4	7.6
<b>0.5 mg/L free chlorine<sup>a</sup></b>					
Free Cl <sup>-</sup> (mg/L)	0.5	0.4	0.4	0.5	1.0
Temperature (°C)	23.6	25.9	23.1	26.9	23.4
pH	7.7	7.4	7.6	7.6	7.7
<b>1.0 mg/L free chlorine</b>					
Free Cl <sup>-</sup> (mg/L)	1.0	1.1	0.9	1.1	1.2
Temperature (°C)	23.2	25.5	23.0	26.8	23.3
pH	7.7	7.8	7.9	7.9	7.9
<sup>a</sup> Pipe loop systems were amended to a target concentration of 1.0 mg/L free chlorine on day 14.					
<sup>b</sup> Days after the addition of $3.0 \times 10^8$ <i>B. globigii</i> spores to each PVC pipe loop system (Time 0 = 10 min).					

The biofilms were characterized by measuring total polysaccharide, free protein, and extracellular nucleic acid concentrations (Table 5). In the chlorine-free, untreated pipe loop, the polysaccharide concentrations increased steadily over the course of the study to a maximum concentration of  $3.6 \mu\text{g}/\text{cm}^2$  after 14 days of circulation. On Day 14, free protein and nucleic acids also accumulated to maximum concentrations of  $0.3 \mu\text{g}/\text{cm}^2$  and  $2.4 \mu\text{g}/\text{cm}^2$ , respectively. Poising the system at 1.0 mg/L free chlorine on Day 14 decreased the polysaccharide concentration to  $1.6 \mu\text{g}/\text{cm}^2$ ; both extracellular proteins and free nucleic acids were completely oxidized after seven additional days of circulation. The biofilms within the chlorine-treated pipe loops remained intact, and no statistical variation in polysaccharide concentrations were observed over the course of the study. This finding was consistent with studies that have demonstrated that free chlorine concentrations less than 5 mg/L have little effect on biofilm stability (Chen and Stewart 2000; Daly et al. 1989). The nearly two-fold decrease in the biofilm composition observed in the untreated pipe loop after the addition of sodium hypochlorite on Day 14 was likely due to detachment caused by sudden environmental stress (Garny et al. 2009).

Table 5. PVC pipe loops, biofilm conditions.

	Time (days) <sup>c</sup>				
	0	3	7	14	21
<b>0.0 mg/L free chlorine<sup>a,b</sup></b>					
Polysaccharide ( $\mu\text{g}/\text{cm}^2$ )	$0.6 \pm 0.1$	$1.2 \pm 0.4$	$1.4 \pm 0.5$	$3.6 \pm 0.5$	$1.6 \pm 0.1$
Protein ( $\mu\text{g}/\text{cm}^2$ )	$0.1 \pm 0.0$	$0.1 \pm 0.0$	$0.2 \pm 0.1$	$0.3 \pm 0.0$	$0.0 \pm 0.0$
Nucleic acids ( $\text{ng}/\text{cm}^2$ )	$0.8 \pm 0.4$	$1.7 \pm 0.7$	$1.1 \pm 0.4$	$2.4 \pm 1.2$	$0.0 \pm 0.0$
<b>0.5 mg/L free chlorine<sup>a,b</sup></b>					
Polysaccharide ( $\mu\text{g}/\text{cm}^2$ )	$0.6 \pm 0.1$	$0.6 \pm 0.2$	$0.8 \pm 0.2$	$0.4 \pm 0.2$	$0.4 \pm 0.2$
Protein ( $\mu\text{g}/\text{cm}^2$ )	$0.1 \pm 0.0$	$0.1 \pm 0.0$	$0.1 \pm 0.0$	$0.1 \pm 0.0$	$0.0 \pm 0.0$
Nucleic acids ( $\text{ng}/\text{cm}^2$ )	$0.0 \pm 0.0$	$0.0 \pm 0.0$	$0.0 \pm 0.0$	$0.0 \pm 0.0$	$0.0 \pm 0.0$
<b>1.0 mg/L free chlorine<sup>a</sup></b>					
Polysaccharide ( $\mu\text{g}/\text{cm}^2$ )	$0.4 \pm 0.1$	$0.4 \pm 0.2$	$0.6 \pm 0.3$	$0.8 \pm 0.2$	$0.6 \pm 0.2$
Protein ( $\mu\text{g}/\text{cm}^2$ )	$0.0 \pm 0.0$	$0.0 \pm 0.0$	$0.0 \pm 0.0$	$0.0 \pm 0.0$	$0.0 \pm 0.0$
Nucleic acids ( $\text{ng}/\text{cm}^2$ )	$0.0 \pm 0.0$	$0.0 \pm 0.0$	$0.0 \pm 0.0$	$0.0 \pm 0.0$	$0.0 \pm 0.0$
<sup>a</sup> Data are means $\pm$ SD ( $n = 3$ ).					
<sup>b</sup> Pipe loop systems were amended to a target concentration of 1.0 mg/L free chlorine on day 14.					
<sup>c</sup> Days after the addition of $4.0 \times 10^8$ <i>B. globigii</i> spores to each PVC pipe loop system (Time 0 = 10 min).					

Free protein remained steady at  $0.1 \mu\text{g}/\text{cm}^2$  in the 0.5 mg/L free chlorine-amended pipe loop, until the chlorine concentration was increased to 1.0 mg/L on Day 14, when proteins were completely oxidized. No proteins or nucleic acids were detected in the 1.0 mg/L free chlorine amended pipe loop throughout the study. Collectively, the biofilm physiological conditions clearly demonstrated the ability of the PVC pipe biofilm to grow under oligotrophic conditions. Furthermore, free chlorine concentrations of 0.5 mg/L were sufficient to penetrate and suppress polysaccharide formation in addition to oxidize nucleic acids; however, free chlorine concentrations greater than 0.5 mg/L were required to completely oxidize biofilm proteins.

The concentrations of heterotrophic bacteria in the bulk water were also monitored. HPCs were conducted on the pipe loop bulk water prior to the addition of sodium hypochlorite, and approximately  $3.4 \times 10^3$  CFUs/mL were observed in each system after flushing with dechlorinated tap water.

Heterotrophs remained stable in the chlorine-free, untreated system until the addition of 1.0 mg/L free chlorine on Day 14 (Figure 15), after which the total number of heterotrophs was below detection after 7 additional days. In the 0.5 mg/L amended pipe loop, heterotrophs decreased  $1.6\text{-log}_{10}$  within the 3-day stabilization period prior to inoculation. No viable HPCs were detected in the 1.0 mg/L free chlorine treated pipe loop throughout the 21-day study, indicating complete inactivation.

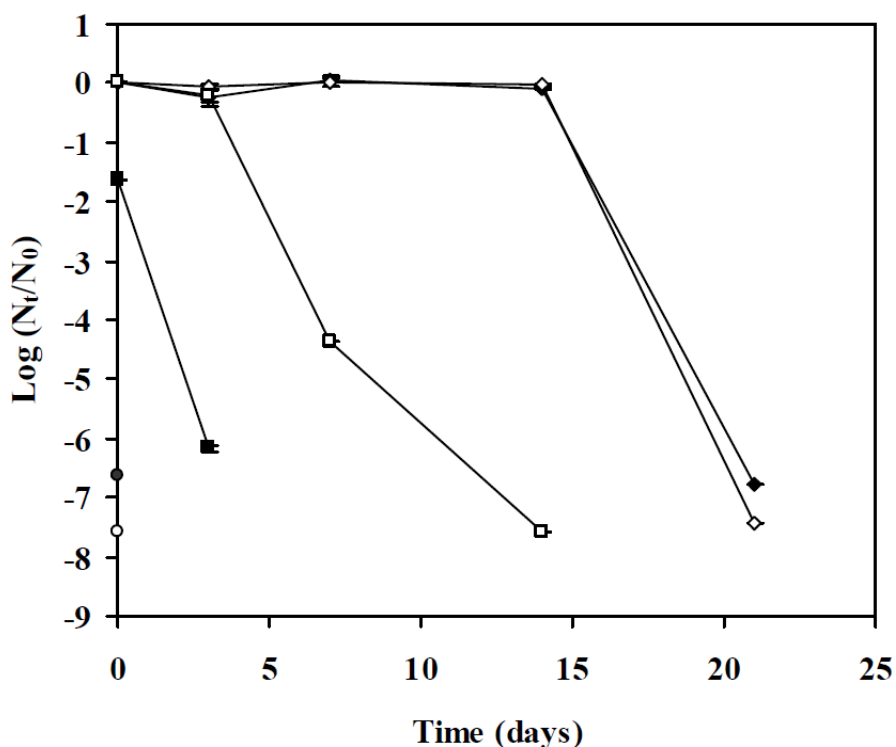


Figure 15. Susceptibility of heterotrophic bacteria and *B. globigii* spores to free chlorine in PVC pipe loop bulk water, presented as the  $\log_{10}$  of the total surviving fraction. Approximately  $3.0 \times 10^8$  viable *B. globigii* spores were added to each pipe loop system on Day Zero. Free chlorine in all systems was poised at 1.0 mg/L on Day 14. (Symbols: ◆ = heterotrophs, chlorine untreated; ◇ = *B. globigii*, chlorine untreated; ■ = heterotrophs, 0.5 mg/L free chlorine; □ = *B. globigii*, 0.5 mg/L free chlorine; ● = heterotrophs, 1.0 mg/L free chlorine; and ○ = *B. globigii*, 1.0 mg/L free chlorine. Data are means  $\pm$  SD ( $n=3$ ); some error bars are not visible due to size.

The concentration of viable *B. globigii* spores in the bulk solution of each pipe was also monitored. In the chlorine-free, untreated pipe, the spore concentration was  $1.5 \times 10^4 \pm 1.2 \times 10^3$  CFUs/mL and remained steady until the introduction of 1.0 mg/L free chlorine on Day 14 (Figure 16). Within seven days of spiking the chlorine, spore viability was reduced to levels below the detection limit. The spore concentration in the 0.5 mg/L pipe loop was  $2.3 \times 10^4 \pm 1.2 \times 10^3$  CFUs/mL after 10 min of circulation. Despite ex-

posure to 0.5 mg/L of chlorine for 10 min, no difference in spore concentration was observed between the untreated and 0.5 mg/L free chlorine amended pipe loops, indicating no inactivation had occurred in the initial timeframe. Subsequently, inactivation of greater than four logs was observed within 14 days. In the pipe loop containing 1.0 mg/L free chlorine, no viable spores were detected within the bulk water throughout the study.

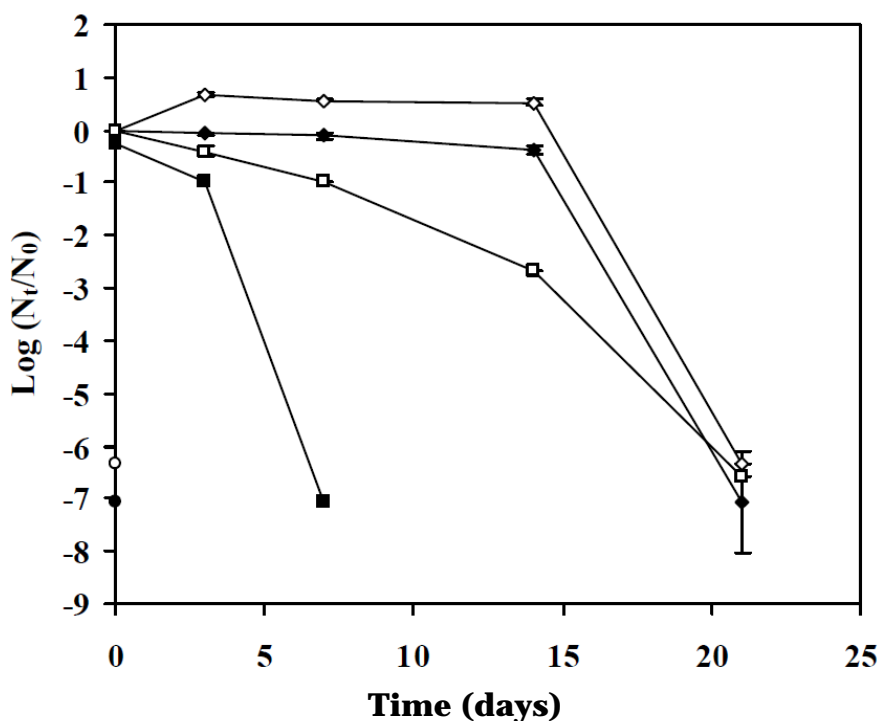


Figure 16. Susceptibility of heterotrophic bacteria and *B. globigii* spores to free chlorine in PVC pipe biofilm, presented as the  $\log_{10}$  of the total surviving fraction. Approximately  $3.0 \times 10^8$  *B. globigii* spores were added to each pipe loop system on day zero. Free chlorine in all systems was poised at 1.0 mg/L on day 14. Symbols: ◆ heterotrophs, chlorine untreated; ◇ *B. globigii*, chlorine untreated; ■ heterotrophs, 0.5 mg/L free chlorine; □ *B. globigii*, 0.5 mg/L free chlorine; ● heterotrophs, 1.0 mg/L free chlorine; and ○ *B. globigii*, 1.0 mg/L free chlorine. Data are means  $\pm$  SD (n=3), some error bars are not visible due to size.

Biofilm HPCs in the chlorine-unamended pipe loop were  $1.4 \times 10^3 \pm 2.2 \times 10^2$  CFUs/cm<sup>2</sup> at the start of the study and remained stable until chlorine treatment (Figure 16). Addition of 1.0 mg/L free chlorine into the non-chlorinated pipe loop resulted in a reduction in HPCs to non-detectable levels within 7 days. A 1.0- $\log_{10}$  reduction in heterotrophs was observed after 3 days circulation in the 0.5 mg/L free chlorine treated pipe loop, and complete inactivation was achieved after 7 days of incubation. Consistent with published studies, sessile heterotrophs were more resistant (nearly 3-

times) to chlorine inactivation than planktonic forms (Murga et al. 2001; Park et al. 2001; Steed and Falkinham 2006; Szabo et al. 2006; DeQueiroz and Day 2007; Bressler et al. 2009). As expected, elevated free chlorine concentrations increased the rate of heterotroph disinfection. As seen with the bulk water, no CFUs were detected within the biofilm of the pipe loop amended with 1.0 mg/L free chlorine throughout the 21-day study, indicating 100% inactivation within the 3 days prior to spore inoculation.

*B. globigii* spores were found to associate rapidly with the pipe surface biofilm. After 10 min of circulation,  $285 \pm 92$  and  $480 \pm 6$  viable spores/cm<sup>2</sup> of pipe and 0.5 mg/L free chlorine loops, respectively, were detected in biofilm samples from the untreated pipe loop (Figure 16). After 3 days of circulation, the number of spores associated with the biofilm in the untreated pipe loop increased to  $1.3 \times 10^3 \pm 205$  spores/cm<sup>2</sup> (0.7-log<sub>10</sub> increase), which represented roughly 3% of the total spores added to the system. An aqueous infective dose is estimated to be 171 spores/L, at a consumption rate of 5 L/day for seven days (Burrows and Renner 1999). Studies have shown that more than 90% of a pipe biofilm can be sloughed from the surface (Garny et al. 2009), suggesting that spore concentrations observed within the PVC pipe biofilm during the current study were theoretically sufficient to cause infection in the event of biofilm detachment.

Spore numbers remained statistically consistent in the untreated pipe loop until the addition of 1.0 mg/L free chlorine to the system on Day 14. After chlorine treatment, *B. globigii* spores were not detected after 7 additional days of circulation, which represented a 7.1-log<sub>10</sub> reduction in the total sessile spore population (Figure 16). In the 0.5 mg/L free chlorine loop system, only a 2.7-log<sub>10</sub> reduction in sessile spores was observed after 14 days of circulation when compared to a decrease below detection in the bulk water phase. This observation indicated a decrease in disinfection efficiency within the biofilm, likely due to protection of enmeshed spores from chlorine (De Beer et al. 1994; Szabo et al. 2006).

Interestingly, the biofilms that developed in both the 0.5 mg/L and the 1.0 mg/L free chlorine pipe loops had approximately equal concentrations of polysaccharides, yet no viable spores were detected within the biofilm of 1.0 mg/L amended pipe loop throughout the study. Light microscopy revealed spores were embedded within the biofilm. The lack of viable spores within the bulk water indicated spores were likely inactivated prior to incorporation into the biofilm. In the 0.5 mg/L free chlorine pipe loop, the

slower inactivation rate allowed viable spores to integrate within the bio-film, which resulted in elevated persistence within the loop system.

Although 1.0 mg/L free chlorine was demonstrated to completely inactivate  $1.8 \times 10^4$  *B. globigii* spores/mL within the PVC pipe systems, it is noted that these experiments were conducted at room temperature, and chlorine inactivation at typical water distribution temperatures is expected to reduce  $\log_{10}$  inactivation ratios appreciably (Ndiongue et al. 2005). Rice et al. (2005) observed approximately a three-fold increase in 2-  $\log_{10}$  inactivation values for *B. anthracis* Sterne and *B. cereus* when temperature was decreased from 23°C to 5°C in the presence of free chlorine. When treated with monochloramine, Rose et al. (2007) reported increased 2- $\log_{10}$  inactivation times of eight-fold for *B. anthracis* Ames and seven-fold for *B. anthracis* Sterne, when temperatures decreased from 25 °C to 5 °C. These reports suggest that spore inactivation intervals for a given  $\log_{10}$  reduction within the pipe loop systems described in this study would increase significantly at lower water temperatures.

## 4 Implementation into EPANet MSX

EPANet is quite uneven in its ability to accept the results of our research. Some capabilities to model applicable ordinary differential equations are built in. For the reaction rates of bacillus species in chlorinated water, the software merely requires a supplemental library from which it can draw kinetic parameters based on the contaminant selected.

For the sorption / desorption model developed through the use of NAMd, a general description of how to derive the ordinary differential equation of interest is based on the form of the function  $f$  is beyond the scope of this document. However, it is instructive to quickly summarize how this is done for our previously measured uptake equation, reproduced here as Equation 15.

$$\frac{P(t)}{C_0} = \beta(1 - e^{-t/\Gamma}) \quad \text{Equation 15}$$

Here we can observe that the system has two components (water and pipe) and that the dynamics are first order (one time constant,  $\Gamma$ ). Hence, we can readily derive the first order, ordinary differential equation governing static sorption and desorption in static conditions, shown by Equation 16.

$$\begin{bmatrix} \dot{C}(t) \\ \dot{P}(t) \end{bmatrix} = \begin{bmatrix} -\beta/\Gamma & (1-\beta)/\Gamma \\ \beta/\Gamma & -(1-\beta)/\Gamma \end{bmatrix} \begin{bmatrix} C(t) \\ P(t) \end{bmatrix} \quad \text{Equation 16}$$

Where

$C(t)$  = contaminant concentration in water

$P(t)$  = the concentration in the pipe wall

$\beta$  = asymptotic uptake and

$\Gamma$  = time constant

The differential equation has eigenvalues at 0 and  $-1/\Gamma$ . The associated eigenvectors are  $[1-\beta, \beta]$  and  $[1, -1]$  respectively. This makes intuitive sense because the first eigenvalue of 0 gives an eigenvector pointing along the the stable equilibrium line in the phase space. This is consistent with thermodynamic partition and predicted by the uptake equation. The se-

cond eigenvalue shows the correct time constant of the system as it moves toward equilibrium. The direction of the second eigenvector forces the system to move along lines in the phase space where  $C(t) + P(t) = \text{constant}$  so that the mass of total contaminant is conserved.

If we were writing the pipe segment hydraulic simulation from scratch, we would then proceed to modify this differential equation to capture water flow and aggregation at the pipe segment level. The resulting differential equation would then be expressed as a difference equation. Having reviewed the source code of EPANet 2.0, these changes appear in the file **quality.c**, in the subroutines **ratecoeffs**, **piperate**, and **wallrate**. EPANet uses a *Lagrangian Time-Drive Method* to calculate system updates. Reaction equations and flow equations are run in alternating sequence, with the spatial size of pipe lengths determined adaptively by creating new lengths when the concentration of a water constituent in adjacent pipe lengths exceeds a fixed threshold.

#### 4.1 Simulations of fate and transport using EPANet MSX

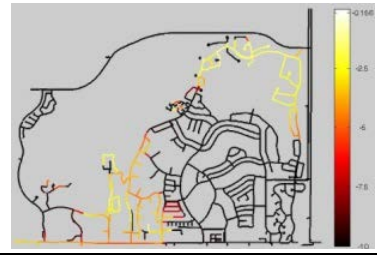



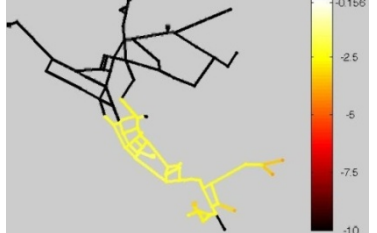

The fate and transport equation above was implemented in EPANet MSX (multi-species extension), which is under development at USEPA's National Homeland Research Center and at the University of Cincinnati. The preamble code is a direct quote of the equation and is given in the following diagram. Rate constants were taken from ERDC-CERL molecular modeling measurements confirmed by laboratory analysis.

As a result, EPANet MSX was able to render animations of simulation results, as shown in Table 6, to clearly show the difference between contaminants that are hydrophilic (easily soluble in water) and those that are hydrophobic (likely to stick to the pipe surface).

When the hydrophobic contaminant sticks to the pipe, the time constants describing uptake and release are significantly longer than time constants describing hydraulic transport. Therefore, the contamination event has an expected duration of weeks, not hours. This duration difference is also summarized in Figure 17..



Table 6. ERDC-developed EPANET MSX physicochemical model simulations, showing the end state after 24 hours of a contamination event in two water distribution system layouts comparing hydrophilic contaminant distribution in water and on pipe walls.

At 24 Hours After Contamination	Hydrophilic Contaminant (concentration in bulk water)	Hydrophobic Contaminant (concentration in bulk water)	Hydrophobic Contaminant (concentration on pipe)
Subdivision (no tanks)			
Mains (with tanks)			

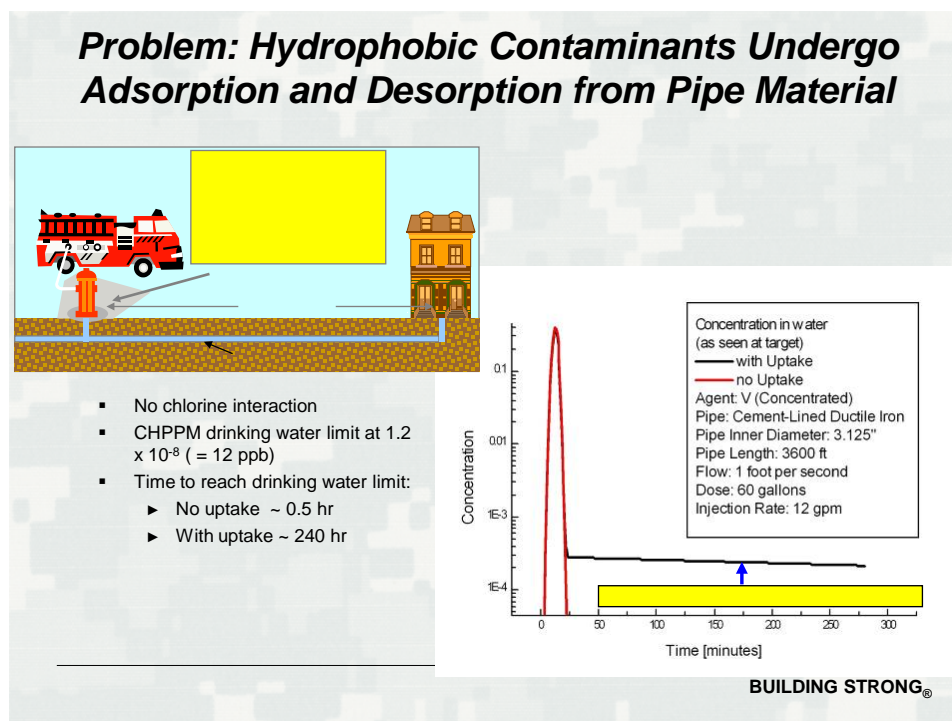


Figure 17. Hydrophilic water contamination would take a matter of hours, not days. Hydrophobic contamination would linger for a number of days.

## 5 Future Research Efforts

### 5.1 Water Integrated Security Test Laboratory

Future goals include expansion and validation of the results obtained from this work, with increased focus on developing an integrated system of protection (Figure 18). There is a need to develop reliable systems with the ability to detect and respond to water contamination in a timely manner to keep water distribution systems protected from intentional and accidental poisoning.

In order to examine the reliability of system components, research on detection, prevention, and mitigation of contamination of water distribution systems in a small scale will be performed at the Water Integrated Security Test Laboratory (WISTL) located at ERDC-CERL Champaign, IL. The WISTL allows replication of different water conditions around the world and simulation of possible water contamination events. Such events will be detected by a real-time early warning system (HACH Homeland Security Technologies Guardian Blue®) and a real-time treatment station with a high-quality, unique filtration system based on *Teslin*®, a synthetic printing medium manufactured by PPG Industries.

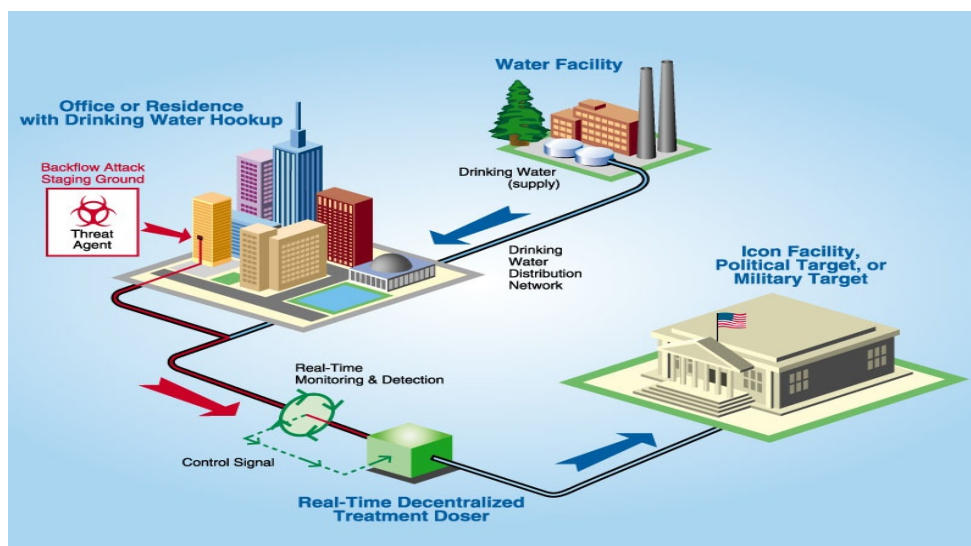


Figure 18. Integrated water system protection.

## 5.2 Secondary aerosol modeling

When a biological warfare attack is launched through aerosolization, the initial contaminant plume is referred to as the *primary aerosol*. The primary aerosol typically accounts for the greatest risk of illnesses and death associated with a biological attack. Under normal circumstances, a biological aerosol can be dispersed and begin to be deposited on surfaces within hours of release, depending on meteorological conditions and spore aerodynamics (Meselson et al. 1994). Evidence suggests that biological agents may be resuspended from the ground or other surfaces (e.g., HVAC ducts) and continue to exist in the atmosphere as a *secondary aerosol* (Inglesby et al. 1999; Weis et al. 2002). Thus, there is potential that persistent secondary aerosols will continue to pose a significant health hazard to building occupants.

Experimental work has been done to characterize the resuspension of particles from various surfaces common to an office building under various flow characteristics (Mukai et al. 2009). While it is useful to do experimental work such as this, it is impossible to fully understand the scope of the problem due to many variables in airflow characteristics as well as differing rates of re-aerosolization among particles of interest. Initial theoretical work has been completed to determine the resuspension term from indoor surfaces as applied to commercially available computational fluid dynamics (CFD) codes (Kim et al. 2010).

While there is significant importance in modeling sorption and desorption of contaminants from pipe walls in an aqueous system, there is equal importance in modeling the same trends in air. Chemical and biological defense is a key focus within the Army, as listed as an Army FY11 Tier 1 Warfighter Outcome. Enhanced protection and decontamination of facilities can be gained by increased understanding of secondary aerosolization of bioaerosols.

Thus, it is important to continue to expand knowledge about particle re-aerosolization, to better understand bioaerosol transport through buildings and the implications of secondary aerosols in decontamination of affected facilities. The use of molecular models described within this report is a promising method to expand this area of knowledge and increase protection and mitigation capabilities for a biological attack.

(This page intentionally left blank.)

## References

- Bressler, D., Balzer, A., Dannehl, A., Flemming, H.-C., & Wingender, J. 2009. "Persistence of *Pseudomonas aeruginosa* in Drinking-Water Biofilms on Elastomeric Material." *Water Science Technology* 9(1): 81–87.
- Carr, Rogan, Jeffrey Comer, Mark D. Ginsberg, and Aleksei Aksimentiev. 2011a. "Atoms-to-Microns Model for Small Solute Transport through Sticky Nanochannels." *Lab on a Chip* 11:3766–3773. doi: 10.1039/c11c20697d.
- \_\_\_\_\_. 2011b. "Modeling Pressure-Driven Transport of Proteins through a Nanochannel." *IEEE Transactions on Nanotechnology* 10 (1): 75.
- Burrows, W. D. and S.E. Renner. 1999. "Biological Warfare Agents as Threats to Potable Water." *Environmental Health Perspectives* 107 (12): 975–984.
- Chen, X. and P.S. Stewart. 2000 "Biofilm Removal Caused by Chemical Treatments." *Water Research* 34 (17): 4229–4233.
- Daly, B., W. B. Betts, A. P. Brown, and J. G. O'Neill. 1989. "Bacterial Loss from Biofilms Exposed to Free Chlorine." *Microbios* 96 (383): 7–21.
- DeQueiroz, G. A., and D. F. Day. 2007. "Antimicrobial Activity and Effectiveness of a Combination of Sodium Hypochlorite and Hydrogen Peroxide in Killing and Removing *Pseudomonas Aeruginosa* Biofilms from Surfaces." *Journal of Applied Microbiology* 103 (4): 794–802.
- Dubois, M., K. A. Gilles, J. K. Hamilton, and P.A. Rebers. 1956. "Colorimetric Method for Determination of Sugars and Related Substances." *Analytical Chemistry* 28: 350–356.
- Garny, K., T. R. Neu, and H. Horn. 2009. "Sloughing and Limited Substrate Conditions Trigger Filamentous Growth in Heterotrophic Biofilms – Measurements in Flow-Through Tube Reactor." *Chemical Engineering Science* 64 (11): 2723-2732.
- Ginsberg, Mark D., Margaret M. Hurley, Aleksei Aksimentiev, Frances C. Hill, and Vincent F. Hock. 2008. "Computational Models to Determine Transport and Hydrolysis Rate Parameters of Contaminants in a Water Distribution System." Presented paper at Army Science Conference held 1-4 December 2008 in Orlando, FL.
- Inglesby, T.V., D.A. Henderson, J.G. Bartlett, M.S. Ascher, E. Eitzen, A.M. Friedlander, J. Hauer, J. McDade, M.T. Osterholm, T. O'Toole, G. Parker, T.M. Perl, P.K. Russell, and K. Tonat. 1999. "Anthrax as a Biological Weapon: Medical and Public Health Management." *JAMA* 281 (18): 1735-1745.
- Kim, Y., A. Gidwani, B.E. Wyslouzil, and C.W. Sohn. 2010. "Source Term Models for Fine Particle Resuspension from Indoor Surfaces." *Building and Environment* 45 (8): 1854–1865.

- Meselson, M., J. Guillemin, M. Hugh-Jones, A. Langmuir, I. Popova, A. Shelokov, and O. Yampoldkaya. 1994. "The Sverdlovsk Anthrax Outbreak of 1979." *Science*. 266 (5188): 1202–1208.
- Morrissey, Kevin M., Theresa R. Connell, William R. Creasy, John R. Stuff, H. DuPont Durst, and Richard J. O'Connor. (February) 1999a. *Qualitative Analysis of Residual VX in Caustic Neutralization Solutions by Solid Phase Extraction and GC/MSD: Analysis of Hydrolysate as Separated Organic and Aqueous Phases*. ECBC-TR-009. Aberdeen Proving Ground, MD: Edgewood Chemical Biological Center of U.S. Army Solider and Biological Chemical Command.
- Morrissey, Kevin M., Theresa R. Connell, John R. Stuff, H. DuPont Durst, and Richard J. O'Connor. (April) 1999b. *Qualitative Analysis of Residual VX in Caustic Neutralization Solutions by Solid Phase Extraction and GC/MSD: Analysis of Hydrolysate as Unseparated Phases*. ECBC-TR-010. Aberdeen Proving Ground, MD: Edgewood Chemical Biological Center of U.S. Army Solider and Biological Chemical Command.
- Mukai, C., J.A. Siegel, and A. Novoselac. 2009. "Impact of Airflow Characteristics on Particle Resuspension from Indoor Surfaces." *Aerosol Science and Technology* 43 (10): 1022–1032.
- Murga, R., T. S. Forster, E. Brown, J. M. Pruckler, B. S. Fields, and R.M. Donlan. 2001. "Role of Biofilms in the Survival of Legionella Pneumophila in a Model Potable Water System." *Microbiology* 147 (11): 3121–3126.
- Ndiongue, S., P. M. Huck, and R. M. Slawson. 2005. "Effects of Temperature and Biodegradable Organic Matter on Control of Biofilms by Chlorine in a Model Drinking Water Distribution System." *Water Research* 39 (6): 953–964.
- Nicholson, W. L., N. Munakata, G. Horneck, H. J. Melosh, and P. Setlow. 2000. "Resistance of Bacillus Endospores to Extreme Terrestrial and Extraterrestrial Environments." *Microbiology and Molecular Biology Reviews* 64 (3): 548–572.
- Park, S. R., W. G. Mackay, and D. C. Reid. 2001. "Helicobacter Sp. Recovered from Drinking Water Biofilm Sampled from a Water Distribution System." *Water Research* 35 (6):1624–1626.
- Rice, E. W., N. J. Adcock, M. Sivaganesan, and L. J. Rose. 2005. "Inactivation of Spores of Bacillus Anthracis Sterne, Bacillus Cereus, and Bacillus Thuringiensis Subsp. Israelensis by Chlorination." *Applied and Environment Microbiology* 71 (9): 5587–5589.
- Rose, L. J., E. W. Rice, L. Hodges, A. Peterson, and M. J. Arduino. 2007. "Monochloramine Inactivation of Bacterial Select Agents." *Applied and Environment Microbiology* 73 (10): 3437–3439.
- Schaeffer, A. B. and M. Fulton. 1993. "A Simplified Method of Staining Endospores." *Science*. 77 (1990): 194.
- Schwartz, T., S. Hoffmann, and U. Obst. 2003. "Formation of Natural Biofilms during Chlorine Dioxide and UV Disinfection in a Public Drinking Water Distribution System." *Journal of Applied Microbiology* 95 (3): 591–601.

- Steed, K. A., and J. O. Falkinham. 2006. "Effect of Growth in Biofilms on Chlorine Susceptibility of *Mycobacterium Avium* and *Mycobacterium Intracellulare*." *Applied and Environment Microbiology* 72 (6): 4007–4011.
- Szabo, J. G., E. W. Rice, and P. L. Bishop. 2006. "Persistence of *Klebsiella Pneumoniae* on Simulated Biofilm in a Model Drinking Water System." *Environmental Science and Technology* 40 (16): 4996–5002.
- Vishnyakov, Aleksey, and Alexander Neimark. 2004. "Specifics of Solvation of Sulfonated Polyelectrolytes in Water, Dimethylmethylphosphonate, and Their Mixture: A Molecular Simulation Study." *Journal of Physical Chemistry A* 108 (8): 1435–1439.
- Weis, C.P., A.J. Intrepido, A.K. Miller, P.G. Cowin, M.A. Durno, J.S. Gebhardt, and R. Bull. 2002. "Secondary Aerosolization of Viable *Bacillus Anthracis* Spores in a Contaminated US Senate Office." *JAMA*. 288 (22): 2853–2858.
- World Health Organization. 2007. "pH in Drinking-water: Revised Background Document for Development of WHO Guidelines for Drinking-water Quality." WHO/SDE/WSH/07.01/1.
- Wright J.B., G.H. Lushington, and M. Hurley. 2005. "Hydrolysis of Phosphorus Esters: A Computational Study." ECBC-TR-434. Aberdeen Proving Grounds, MD: Edgewood Chemical Biological Center—US Army Research, Development and Engineering Command.

## Abbreviations

Term	Description
3-D	three-dimensional
ARL	Army Research Laboratory
BD	Brownian dynamics
C2	Command and Control Centers
CB	chemical-biological
CC	computational chemistry
CFD	computational fluid dynamics
CFU	colony forming unit
CHARMM	Chemistry at HARvard Macromolecular Mechanics; a molecular simulation program with broad application to many-particle systems
CLDI	concrete-lined ductile iron
COA	courses of action
COCOM	Combatant Command
CPCM	polarizable continuum model
cPVC	chlorinated polyvinyl chloride
DMMP	dimethyl-methylphosphonate
DNA	deoxyribonucleic acid
DoD	Department of Defense
DPD	diethyl-p-phenylenediamine
ECBC	Edgewood Chemical and Biological Center
EPANet	A public-domain hydraulic analysis package for water supply networks; developed and maintained by the USEPA
ERDC	Engineer Research and Development Center
G-SMD	grid-steered molecular dynamics
HPC	heterotrophic plate count
LC/MS	liquid chromatography/mass spectrometry
MD	molecular dynamics
MOU	memorandum of understanding
NAMD	Nanoscale Molecular Dynamics
OP	organophosphate
PCM	Polarizable Continuum Model
PMF	potential of mean force
PS	pipe segment
P-S	phosphorus-sulfur
PVC	polyvinyl chloride
RNA	ribonucleic acid
SD	standard deviation
SiO <sub>2</sub>	silica
TSA	tryptic soy agar
TST	Transition State Theory
UIUC	University of Illinois at Urbana-Champaign



Term	Description
USEPA	US Environmental Protection Agency
WISTL	Water Integrated Security Test Laboratory

REPORT DOCUMENTATION PAGE				Form Approved OMB No. 0704-0188	
Public reporting burden for this collection of information is estimated to average 1 hour per response, including the time for reviewing instructions, searching existing data sources, gathering and maintaining the data needed, and completing and reviewing this collection of information. Send comments regarding this burden estimate or any other aspect of this collection of information, including suggestions for reducing this burden to Department of Defense, Washington Headquarters Services, Directorate for Information Operations and Reports (0704-0188), 1215 Jefferson Davis Highway, Suite 1204, Arlington, VA 22202-4302. Respondents should be aware that notwithstanding any other provision of law, no person shall be subject to any penalty for failing to comply with a collection of information if it does not display a currently valid OMB control number. <b>PLEASE DO NOT RETURN YOUR FORM TO THE ABOVE ADDRESS.</b>					
1. REPORT DATE (DD-MM-YYYY) May 2012		2. REPORT TYPE Final Technical Report		3. DATES COVERED (From - To)	
4. TITLE AND SUBTITLE Molecular Modeling of Chem-Bio (CB) Contaminant Sorption/Desorption and Reactions in Chlorinated Water Systems				5a. CONTRACT NUMBER	
				5b. GRANT NUMBER	
				5c. PROGRAM ELEMENT NUMBER 21 2040 622784T41	
6. AUTHOR(S) Mark D. Ginsberg, Vincent F. Hock, Margaret Hurley, Frances Hill, Aleksei Aksimentiev, Rogan C. Carr, Jeffrey R. Comer, Kathryn A. Guy, Anne Beckman, Melixa Rivera-Sustache, Andy Nelson, Martin Page, Amanda Ehmann, and Vicki L. Van Blaricum				5d. PROJECT NUMBER 150162	
				5e. TASK NUMBER	
				5f. WORK UNIT NUMBER	
7. PERFORMING ORGANIZATION NAME(S) AND ADDRESS(ES) U.S. Army Engineer Research and Development Center (ERDC) Construction Engineering Research Laboratory (CERL) PO Box 9005 Champaign, IL 61826-9005				8. PERFORMING ORGANIZATION REPORT NUMBER ERDC TR-12-16	
9. SPONSORING / MONITORING AGENCY NAME(S) AND ADDRESS(ES) Headquarters US Army Corps of Engineers 441 G Street NW Washington DC 20314-1000				10. SPONSOR/MONITOR'S ACRONYM(S) USACE	
				11. SPONSOR/MONITOR'S REPORT NUMBER(S)	
12. DISTRIBUTION / AVAILABILITY STATEMENT Approved for public release; distribution is unlimited.					
13. SUPPLEMENTARY NOTES					
14. ABSTRACT Army installations contain a high density of mission-critical buildings that require constant protection from accidental or deliberate contamination of water distribution systems. Current simulations of contaminant fate and transport in pipe systems do not accurately portray reality. The simulations assume pure hydraulic transport of contaminants and do not account for sorption of the contaminant on pipe walls. Additionally, subsequent reactions such as hydrolysis are not considered. These omissions reduce predictability of a contaminant's progression and effect in the distribution system. In addition, inadequate understanding of contaminant fate and transport may result in an unacceptable risk to mission readiness. However, performing laboratory tests for every known and emerging chemical or biological contaminant to obtain uptake and reaction parameters is not feasible with regard to time or cost investments. This report documents advances in molecular modeling predictions for the transport of contaminants using: the Nanoscale Molecular Dynamics program, the influence of bacterial biofilms on spore viability within a chlorinated water distribution system, the computational chemistry predictions of the rate of hydrolysis of a specific contaminant, and the inclusion of results into the predictive software, EPANet. This work opens the way for better vulnerability assessments, protection, real-time response, remediation, and planning.					
15. SUBJECT TERMS chem-bio (CB) contaminants, hydraulic modeling, molecular modeling, water distribution systems, water quality, EPANet					
16. SECURITY CLASSIFICATION OF:			17. LIMITATION OF ABSTRACT  UU	18. NUMBER OF PAGES  58	19a. NAME OF RESPONSIBLE PERSON
a. REPORT Unclassified	b. ABSTRACT Unclassified	c. THIS PAGE Unclassified			19b. TELEPHONE NUMBER (include area code)